NASA TM-83754

Nonlinear Analysis for High-Temperature Multilayered Fiber Composite Structures

Dale A. Hopkins
Lewis Research Center
Cleveland, Ohio

August 1984

NASA

TABLE OF CONTENTS

	Page
LIST OF SYMBOLS	iii
CHAPTER	
1. INTRODUCTION	1
1.1 Background	2
1.2 Problem Definition, Research Objective and Approach	5
2. THEORY	9
2.1 Introduction	9
2.2 Basic Concepts	10
2.2.1 Linear Formulation	10
2.2.2 Nonlinear Analysis	12
2.2.3 Analysis of a Composite . . .	14
2.3 An Integrated Approach	15
2.3.1 Fiber Degradation	18
2.3.2 Nonlinear Thermoviscoplastic Material Behavior	20
2.3.3 Composite Micromechanics . . .	24
2.3.4 Laminate Theory	37

	Page
3. COMPUTER IMPLEMENTATION	49
3.1 Introduction	49
3.2 COBSTRAN Overview	50
3.3 Development of Nonlinear COBSTRAN . . .	52
3.3.1 Fiber Degradation Model . . .	52
3.3.2 Nonlinear TVP Material Relationships	53
3.3.3 Composite Micromechanics Equations	54
3.3.4 Material Failure Theory . . .	55
3.3.5 Geometry Updating	56
3.3.6 Convergence Criterion	57
3.3.7 General Flowchart	58
4. DEMONSTRATION PROBLEM	60
4.1 Introduction	60
4.2 TFRS Turbine Blade Component	62
4.3 Nonlinear COBSTRAN Analyses	65
4.3.1 Simulated Fabrication Process	65
4.3.2 Simulated Engine Mission . . .	80
5. SUMMARY	101
REFERENCES	105
APPENDIX	108

LIST OF SYMBOLS

SYMBOL	
A	Laminate axial stiffness
B	Strain-displacement relationships
C	Structural damping, fiber/matrix interaction constant, heat capacity, laminate coupled stiffness
C_1, C_2, C_3	Constant material parameters
D	Fiber diameter, laminate bending stiffness
e	Exponential function
E	Stress-strain relationships, normal modulus
F	Nodal forces
G	Shear modulus
h	Laminate thickness, perpendicular distance from laminate midplane
I	Identity matrix
k	Constituent volume fraction
K	Structural stiffness, fiber/matrix interaction constant, thermal conductivity
ℓ	Constant material parameter
L	Length
m	Constant material parameter

SYMBOL	
M	Structural mass, laminate moment resultants
M_T	Laminate thermal moment resultants
n	Constant material parameter
N	Laminate stress resultants
N_M	Mechanical load cycles
N_T	Thermal load cycle, laminate thermal stress resultants
P	Material property
Q	Laminate shear stress resultants
R	Penetration of reaction zone for fiber degradation, ply rotation matrix
S, S_C, S_F	Actual, cumulative and fracture strength, respectively
t	Time
T, T_M	Actual and melting temperature, respectively
u	Nodal displacement
x, y, z	Structural coordinate axes
0	Null vector
1, 2, 3	Ply material coordinate axes
α	Thermal expansion coefficient
β	Empirical ply strength constant
δ	Deflection
Δ	Increment
ε	Strain
θ	Ply orientation angle
κ	Laminate curvature

SYMBOL	
λ	Eigenvalues
ν	Poisson's ratio
ρ	Weight density
σ	Stress
ω, ω_n	Actual and natural frequency, respectively

SUBSCRIPT	
a	Actual value
c	Composite or laminate property
cr	Critical value
C	Compression
d	Interphase property
f	Fiber property
H	Highest value
ℓ	Ply or lamina property
m	Matrix property
S	Shear
T	Tension
x, y, z	Structural coordinate axes reference
0	Reference value
1, 2, 3	Ply material coordinate axes reference

SUPERSCRIPT	
A, B, C	Regions of intralaminar nonuniformity
0	Laminate midplane reference

CHAPTER 1

INTRODUCTION

A major thrust of current aeropropulsion research is directed at improving the performance, efficiency, and durability of aircraft gas turbine engines. One specific area of research where efforts are focused concerns the potential use of advanced high-temperature composite materials in critical turbine engine applications. The turbine engine applications of concern here are the components which operate in the hot section of the engine. The blades and vanes of the high-pressure turbine (HPT) are of specific concern in that the temperature-limited capability of current turbine blade/vane materials is a key factor affecting the ability to augment engine performance/efficiency and at the same time enhance, or at least maintain, component durability. In order to examine the feasibility of using advanced high-temperature composite materials for turbine engine components such as HPT blades/vanes, better analytical tools are needed with the capability to account for the complex physics associated with such applications including; nonlinear

(stress-temperature-time dependent) and anisotropic material behavior, microscopic and macroscopic heterogeneity, and fiber degradation. The subject of this thesis is the research conducted, to date, toward the development of such an analytical capability.

1.1 Background

The performance/efficiency characteristics of a gas turbine engine are directly proportional to the engine operating cycle temperature such that the ability to increase the maximum cycle temperature can result in significant improvements to engine performance/efficiency. On the other hand, engine operating cycle temperature is limited by the useful life associated with the materials currently used for engine hot-section components such as HPT blades/vanes. Useful life can be thought of here as the time limit for which a material can be considered reliable in a specific application, hence a measure of component durability. The materials currently used in HPT blade/vane components include mostly nickel- and cobalt-based monolithic superalloys. The possibility for improving engine performance/efficiency without negatively affecting component durability would be greatly enhanced by the ability to improve the elevated temperature capability of turbine blade/vane component materials.

In the past, increases in turbine engine maximum cycle temperature have been accomplished primarily in two ways. First, a general improvement in the properties of nickel- and cobalt-based monolithic superalloys has been achieved through advances in metallurgical processing technology such as directional solidification, oxide dispersion strengthening, and most recently, single crystal formation. This general improvement in properties has, in turn, enhanced the elevated temperature performance of these materials in engine hot-section applications. Second, engines have been designed to operate at turbine inlet gas temperatures approaching the homologous melting point of these conventional turbine blade superalloy materials. Designing engines to operate at these higher temperatures has required the use of complex cooling schemes to divert increased amounts of compressor discharge air to cool the various components. Diverting compressor discharge air for cooling purposes is parasitic to engine performance/efficiency. Moreover, further technological improvement of conventional turbine blade/vane materials seems highly unlikely. It would seem, then, that the key to maximizing turbine engine operating cycle temperature, thereby improving engine performance/efficiency, lies in the ability to develop materials possessing substantially better capabilities for

the extended service, elevated temperature environment typical of HPT blade/vane components.

The challenge to find superior materials for long-term, high-temperature turbine engine applications has, in part, been responsible for the development of a class of materials commonly referred to as "advanced high-temperature composites." Tungsten-fiber-reinforced superalloys (TFRS) are one family of advanced high-temperature composites which have recently been investigated (refs. 1-3) as a potential alternative to conventional monolithic superalloys for use in HPT blade/vane components. Moreover, a specific TFRS composite, namely $WThO_2$-fiber-reinforced FeCrAlY, has been identified (ref. 4) as a viable candidate for a first-generation composite turbine blade/vane material by virtue of the excellent combination of complementary properties provided by this fiber/matrix system. Increases in maximum operating cycle temperature of as much as 200°F have been predicted (ref. 5) for engines having composite HPT blades/vanes of TFRS. In addition, studies (refs. 4, 6) have shown that fabrication of TFRS turbine blade/vane components is feasible and cost-competitive with corresponding monolithic superalloy components. It would appear, at least from a qualitative standpoint, that the benefit represented by the application of TFRS composites to aircraft engine HPT components is evident.

1.2 Problem Definition, Research Objective and Approach

Despite the promising outlook, a dilemma exists regarding the use of TFRS composites in aircraft gas turbine engines. The dilemma concerns the lack of methods available to adequately investigate the feasibility of using TFRS (or any advanced high-temperature composite material) in a specific engine application. For example, any present attempt to assess the performance of a WThO_2-fiber-reinforced FeCrAlY HPT blade/vane component would probably require experimental full-scale engine evaluations. Considering all the variables involved, such an investigation (assuming it was even possible) would be economically prohibitive. The need exists for an analytical capability with which to make a quantitative assessment of the mechanical performance and structural integrity of advanced high-temperature composites in turbine engine applications.

In view of the above-mentioned need, the objective of this research has been to develop a structural/stress analysis capability specifically tailored for the nonlinear analysis of TFRS composite turbine blade/vane structures. Development of this specialized capability has been based on an integrated approach which, in itself, is completely general. As will be seen, the strategy of

this integrated approach provides the conceptual framework whereby specialized analytical capabilities can be developed for any composite structural application.

From the outset, the emphasis in developing this specialized structural/stress analysis capability has been to incorporate the physics governing this particular application into the analytical formulation of the problem. The blade/vane components of the HPT section operate in a severe environment subjecting them to complex and cyclic thermomechanical loading conditions. These loads give rise to highly nonlinear material behavior which, in turn, results in an induced material anisotropy. This problem is further complicated by the local and global inhomogeneity inherent in a fiber-reinforced, multilayered composite structure. Finally, in the long-duration high-temperature environment of a HPT blade/vane, TFRS composites are subject to fiber degradation. As will be discussed in more detail later, fiber degradation is a common phenomenon in certain families of advanced high-temperature composites operating under such conditions.

In the development of a nonlinear structural analysis capability for TFRS composite HPT blade/vane components, the COBSTRAN (COmposite Blade STRuctural ANalysis) computer code was used as a foundation.

COBSTRAN is a structural analysis software system developed at the NASA Lewis Research Center as an in-house research tool to perform linear-elastic structural analysis for composite blade structures. In essence, the present effort has resulted in a "nonlinear" version of COBSTRAN which incorporates the appropriate fiber degradation model, nonlinear thermoviscoplastic material relationships, composite micromechanics theory, laminate theory, and global structural analysis to relate the global structural response of a HPT blade/vane component to the nonlinear behavior of the TFRS constituent materials.

Finally, development of nonlinear COBSTRAN was undertaken as an evolutionary task. As a future effort, it is intended that the capability represented by nonlinear COBSTRAN be "fine-tuned" through an iterative process of empirical investigation and analytical methodology refinement. In this process, nonlinear COBSTRAN will be used as a research tool to conduct parametric/sensitivity studies to isolate critical factors affecting the behavior of TFRS composites in a HPT blade/vane application. Information from the parametric/sensitivity studies will be used to design appropriate experimental investigations to further examine physical phenomena that warrant accountability in a

structural analysis. The result of this fine-tuning process will be a validated nonlinear structural analysis/design capability for TFRS composite turbine blade/vane structures.

CHAPTER 2

THEORY

2.1 Introduction

The purpose of this chapter is two-fold. First, an attempt is made to give meaning to the concept of nonlinear analysis for composite structures within the context of how the problem is approached here. The major theoretical aspects involved in this approach are summarized and include; the global formulation of a linear structural analysis problem, the incremental/iterative application of this linear formulation in a nonlinear analysis, and the necessary extensions required for the purpose of analyzing a composite structure. A "composite structure" here implies a multilayered structure composed of unidirectional fiber-reinforced composite plies. Second, a unique approach to nonlinear structural analysis for TFRS composite HPT blade/vane components is presented, followed by a brief discussion of the key elements comprising the approach for this particular application.

2.2 Basic Concepts

2.2.1 Linear Formulation

From a finite element method (FEM) point of view, the global formulation of a linear structural analysis problem (assuming solution by the displacement method) might be summarized by the matrix expressions shown in Figure 1. Admittedly, this small collection of equations represents a rather superficial overview of the finite element method of structural analysis. Nevertheless, the equations in Figure 1 are representative of the governing equations of structural analysis/design as implemented in any general purpose finite element structural analysis computer code.

The first expression in Figure 1 represents the system of differential equations of motion for a discretized structure. In this expression; [M], [C] and [K] represent the global structural mass, damping, and stiffness matrices, respectively, and $\{u\}$, $\{\dot{u}\}$, $\{\ddot{u}\}$ and $\{F(t)\}$ are column vectors that denote the nodal displacements, velocities, accelerations, and applied loads, respectively. The second and third expressions in Figure 1 summarize the eigenvalue problems corresponding to static buckling and free vibration analyses, respectively. In these expressions: λ are the eigenvalues associated with the solutions of each problem; [I] and {0} are the identity matrix and null column vector,

$$[M]\{\ddot{u}\} + [C]\{\dot{u}\} + [K]\{u\} = \{F(t)\}$$

$$\langle [K] - \lambda [I] \rangle \{u\} = \{0\} \rightarrow \{S_{cr}\}$$

$$\langle [K] - \lambda [M] \rangle \{u\} = \{0\} \rightarrow \{\omega_n\}$$

$$\{u\} \leq \{u_a\}$$

$$\{\sigma\} = [E][B]\{u\} \leq \{S_a\}$$
$$\leq \{S_{cr}\}$$

$$\{\omega\} \leq \{\omega_a\}$$

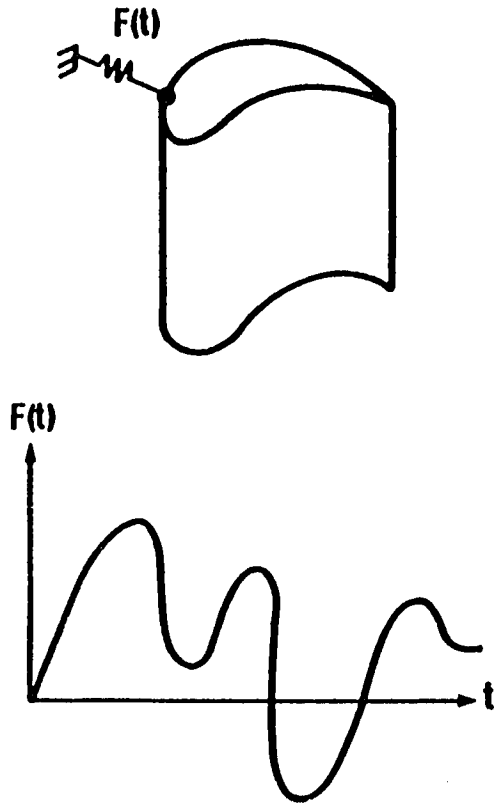

Figure 1 - Summary of Governing Equations of Linear FEM Structural Analysis

respectively, and; $\{S_{cr}\}$ and $\{\omega_n\}$ are the critical buckling loads and natural frequencies, respectively, corresponding to the eigenvalue solutions of the two problems. The last three expressions in Figure 1 indicate the variables commonly of interest (often in comparison to some allowable or critical values) when performing a structural/stress analysis. In these expressions: $\{\sigma\}$ is the column vector of element stresses; [E] and [B] are the stress-strain and strain-displacement relationship matrices, respectively; $\{S_a\}$ and $\{S_{cr}\}$ are the allowable stresses and critical stresses, respectively, and; $\{\omega\}$ and $\{\omega_a\}$ are the actual frequencies and allowable frequencies, respectively.

Although the formulation summarized above is for a general linear structural analysis problem, it can be applied in the nonlinear analysis of a structure, as described in the following section.

2.2.2 Nonlinear Analysis

In the context of this discussion, the global finite element formulation for a linear structural analysis can serve as the basis for a nonlinear structural analysis. For a nonlinear analysis, however, the linear formulation is applied in an incremental/iterative

manner. This approach allows for the fact that many of the terms comprising the governing equations (such as those in Figure 1) are not constant over the range of solution for the problem, but are actually dependent functions of certain solution variables.

In applying this incremental/iterative approach, the solution of a nonlinear structural analysis problem is treated as an iterative process that involves "marching out" in time and performing the analysis (i.e., solving the linear problem formulation) for distinct load/time increments of the total range of solution for the problem. Furthermore, as the iterative solution process progresses, the results from the analysis of each step or increment are used to modify or update various aspects of the problem formulation for the analysis of each successive increment. Interpretation of the physical phenomena governing the particular structural application dictates which aspects of the analytical formulation of the problem are modified during the solution process, as well as the methodologies on which these modifications are based. In the case of a structural analysis involving material nonlinearity, for example, the modification methodology might include a constitutive relationship which "models" the nonlinear material behavior due to factors such as temperature, inelastic strain, fatigue, and creep.

In theory, the general formulation presented above is directly applicable to the analysis of a composite structure. However, in most finite element computer codes, this formulation is implemented in such a way that certain extensions are required for the purpose of analyzing a composite structure.

2.2.3 Analysis of a Composite

In principle, the finite element formulation of a structural analysis problem, as summarized earlier, does not preclude inhomogeneity of the elements comprising a discretized structure. In reality, however, very few finite element computer codes will accommodate, directly, the macroscopic heterogeneity inherent in a composite structure. Moreover, a multilayered fiber-reinforced composite structure is heterogeneous in both a microscopic and macroscopic sense. As a consequence, there are certain aspects which distinguish the analysis of a composite structure from the analysis of an ordinary homogeneous structure.

The distinguishing features involved in the analysis of a composite structure include the additional theories and assumptions employed to represent the inherently heterogeneous composite structure as an equivalent "pseudo-homogeneous" structure. As will be

seen, in the approach taken here for nonlinear structural analysis of TFRS composite HPT blade/vane components, these additional theories provide for the generation of the various global structural properties and degeneration of the global field variables during the incremental solution process. These aspects, unique to the analysis of a composite structure, involve such subjects as composite micromechanics theory and laminated plate theory and are discussed in more detail to follow.

2.3 An Integrated Approach

The approach taken here for the nonlinear structural analysis of TFRS composite HPT blade/vane components is shown schematically in Figure 2. This approach is referred to as an "upward-integrated top-down-structured" analysis. The schematic in Figure 2 illustrates the hierarchical levels of integration involved in the nonlinear analysis of a composite structure by this approach. For the special case of a TFRS composite HPT blade/vane component, the key elements comprising this upward-integrated top-down-structured analysis, as shown in Figure 2, include; a fiber degradation model, nonlinear thermoviscoplastic constituent material model, composite micromechanics theory, laminate theory, and global structural analysis.

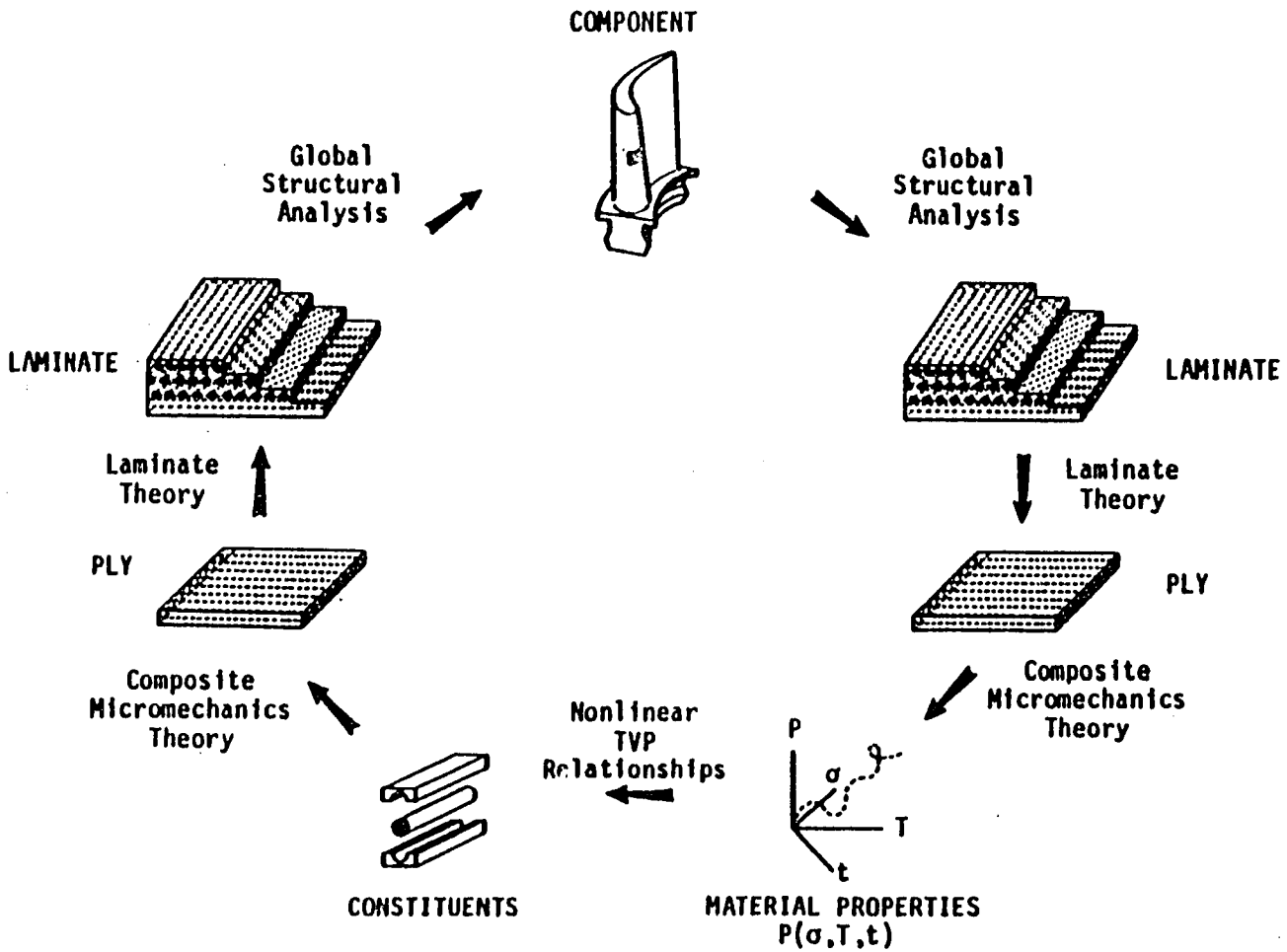

Figure 2 - Upward-Integrated Top-Down-Structured Approach for Composite Structural Analysis

The circular arrangement of Figure 2 is intended to illustrate the incremental/iterative solution strategy imbedded in the upward-integrated top-down-structured approach. As will be discussed later, this incremental/iterative solution strategy involves iteration at two levels. A primary level of iteration occurs for the load/time increments of the total range of solution of the problem. For each load/time increment, a secondary level of iteration occurs to establish equilibrium (in an integrated sense) of the global structural response and thus achieve a convergent solution for the particular load/time increment.

It is worthy of mention again that the upward-integrated top-down-structured approach itself, as illustrated in Figure 2, is general and as such is applicable to the analysis of virtually any composite structure. The individual elements comprising this approach are dependent on the particular composite structural application. Following is a discussion of the key elements comprising the upward-integrated top-down-structured approach for the analysis of a TFRS composite HPT blade/vane component.

2.3.1 Fiber Degradation

Fiber degradation, as previously mentioned, is a metallurgical phenomenon common in the refractory-fiber metal-matrix class of advanced high-temperature composites when used in long-duration high-temperature applications. Generally speaking, the phenomenon involves a chemical reaction at the fiber-matrix interface of a composite lamina. The exact nature and extent of the degradation process is dependent on the particular combination of fiber and matrix in the composite system (see ref. 7). For example, in the case of $WThO_2$-fiber-reinforced FeCrAlY, the fiber degradation mechanism has been characterized (ref. 3) as a recrystallization and partial dissolution induced by the diffusion of matrix material into the fiber. The result of this degradation process is the creation of an interphase of material at the original fiber/matrix boundary.

Depending on the propensity for a particular fiber/matrix system to interact and the character of the resulting interphase of material, the fiber degradation phenomenon can have a significant deteriorating effect on the properties of the composite. Figure 3 illustrates the fiber degradation process for TFRS composites and gives the empirical expression (ref. 4) used to account for and quantify the fiber degradation phenomenon in the analysis

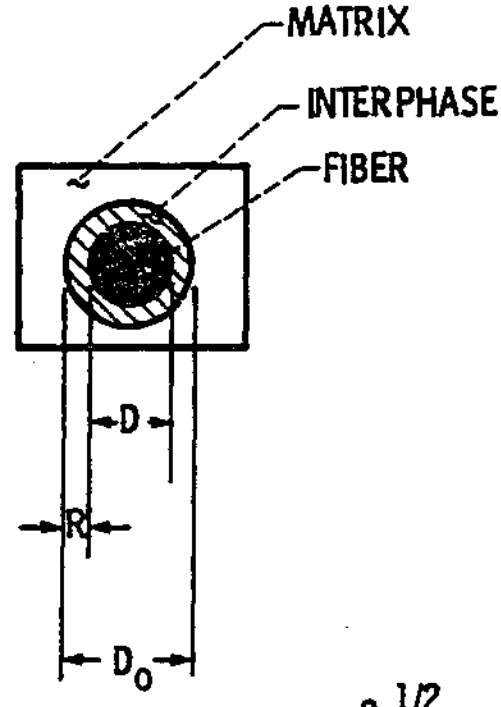

Figure 3 - Schematic and Empirical Expression for Fiber Degradation in TFRS Composites

of a TFRS composite HPT blade/vane component. In the expression: R denotes the incremental penetration of the reaction zone or interphase; R_o represents an initial or reference penetration (resulting, perhaps, from a fabrication process); T denotes the exposure temperature; t denotes the incremental time duration of exposure, and; C and K represent empirical interaction constants for the specific fiber/matrix system.

2.3.2 Nonlinear Thermoviscoplastic Material Behavior

As pointed out earlier, the severe operating environment of a HPT blade/vane component gives rise to highly nonlinear material behavior. In the case of TFRS composites, this material nonlinearity is assumed to be attributable to a stress-temperature-time dependency of the constituent (fiber/matrix/interphase) material properties. In order to account for or model the material nonlinearity in a structural analysis, the nonlinear thermoviscoplastic (TVP) relationships (see Figure 4) proposed by Chamis (ref. 8) have been adopted for the purpose of updating the TFRS constituent material properties of each ply in the multilayered turbine blade/vane component at each iteration during the nonlinear analysis solution process. Although the constituent materials (fiber/matrix) may initially be

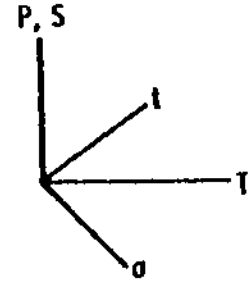

MECHANICAL PROPERTY:

$$P = \left[\frac{T_M - T}{T_M - T_0}\right]^n \left[\frac{S_F - \sigma}{S_F - \sigma_0}\right]^m \left[\frac{\dot{\sigma}_H - \dot{\sigma}_0}{\dot{\sigma}_H - \dot{\sigma}}\right]^\ell (P_0)$$

THERMAL PROPERTY:

$$P = \left[\frac{T_M - T_0}{T_M - T}\right]^n \left[\frac{S_F - \sigma_0}{S_F - \sigma}\right]^m \left[\frac{\dot{\sigma}_H - \dot{\sigma}}{\dot{\sigma}_H - \dot{\sigma}_0}\right]^\ell (P_0)$$

RESIDUAL STRENGTH:

$$S = \left\{\left[\frac{T_M - T}{T_M - T_0}\right]^n - C_1 \log_{10}(N_M) - C_2 \log_{10}(N_T) - C_3 \log_{10}(t)\right\} (S_0) - S_c$$

Figure 4 - Nonlinear TVP Material Relationships

isotropic, the nonlinear material behavior arising from the complex and cyclic thermomechanical loading experienced by a HPT blade/vane results in an induced anisotropy of the constituents.

As shown in Figure 4 the nonlinear TVP expressions provide a relationship between the current (P, S) and reference (P_o, S_o) value of a material property in terms of the current and reference state of the constituent material as described by the indicated field variables. In the relationships: T, T_o, and T_M denote current, reference, and melting temperatures, respectively; S_F denotes fracture strength; σ and σ_o denote current and reference stress, respectively; $\dot{\sigma}$, $\dot{\sigma}_o$, and $\dot{\sigma}_H$ denote current, reference, and maximum allowable stress rates, respectively; N_M and N_T represent the number of mechanical and thermal load cycles, respectively; S_C represents cumulative strength, and; n, m, ℓ, C_1, C_2, and C_3 are empirical material parameters. The constituent material properties which are modified include; normal moduli (E_{11}, E_{22}), average heat capacity (C), thermal conductivities (K_{11}, K_{22}), thermal expansion coefficients (α_{11}, α_{22}), and ultimate strengths (S_{11}, S_{22}, S_{12}). It was assumed here that the Poisson's ratios (ν_{12}, ν_{23}) of a constituent material remain constant and that, for any

given increment, the constituent materials behave in a transversely isotropic manner (isotropic within a plane). The heat capacity and thermal conductivities have been included here in the event that a structural analysis might involve a thermal (heat transfer) analysis in addition to a stress analysis. The ultimate strength properties have been included to accommodate the application of a failure criterion for design purposes.

The relationships in Figure 4 have several attractive features. First, the expressions are of relatively simple form. Second, the relationships are based on commonly used and readily determined variables. Due to these two features, the nonlinear TVP relationships are conducive to implementation in a structural analysis computer code. Third, the relationships are modular, meaning each nonlinear effect or dependency is isolated in a distinct term. This feature would facilitate expansion of the relationships to include the effects of other nonlinear material dependencies (hygral effects, for example). Finally, as a result of their modularity, the relationships are tractable, meaning it is possible to monitor the relative influence of each separate nonlinear dependency from the local behavior of the constituent to the global response of a structure. This tractability feature is useful for the purpose of conducting

sensitivity analyses, as alluded to earlier, to isolate the critical factors controlling a specific problem which might warrant further experimental investigation.

These particular nonlinear TVP material relationships are presented here with the realization that they do not represent an exact or complete mathematical model for describing the full spectrum of nonlinear material behavior possible in a composite structure. What these relationships do represent is simply an attempt to account for the physics involved in the application of TFRS composites for a specific engine component (HPT blade/vane) by incorporating the factor judged to be most critical, namely, stress-temperature-time dependent material nonlinearity. Furthermore, the use of these nonlinear TVP relationships in the upward-integrated top-down structured approach taken here represents an attempt to treat the problem of composite material nonlinearity at the most fundamental level, i.e., in the constituents.

2.3.3 Composite Micromechanics

In short, composite micromechanics is the branch of composite mechanics which provides the formal structure to relate the behavior of a composite lamina or ply to the behavior of the constituents of the ply. For example,

various micromechanistic approaches have been taken to derive equations which predict the material properties of a composite lamina based on the properties of the individual constituents of the composite and the geometrical structure of the lamina (see refs. 9-11, for example).

Recently, simplified composite micromechanics equations have been proposed by Chamis (refs. 12-14) to predict: the material properties (mechanical, thermal, and uniaxial strength) of a unidirectional fiber-reinforced lamina based on the corresponding properties of the constituent materials, and; the distribution of microstresses in the constituent materials resulting from the stress state occurring in a lamina. Similar equations, based on those of Chamis, were derived to account for the existence of an interphase of material at the fiber/matrix boundary, as might result from the fiber degradation phenomenon expected to occur in a TFRS composite HPT blade/vane component.

The coordinate axis system used to define the material properties of a unidirectional fiber-reinforced lamina is shown in Figure 5. The composite micromechanics equations for predicting lamina mechanical properties are shown in Figure 6. Similarly, composite micromechanics equations for predicting lamina thermal properties and

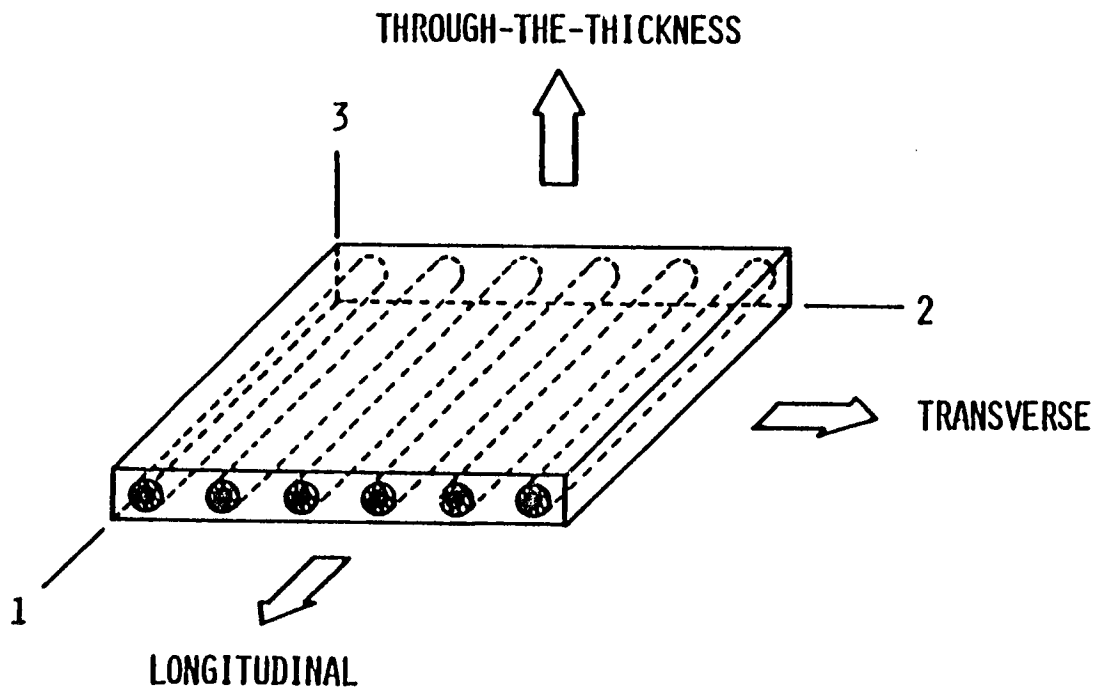

Figure 5 - Definition of Ply Material Coordinate System

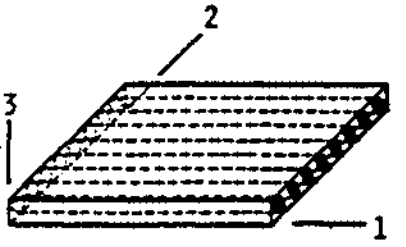

$$E_{\ell 11} = k_m E_{m11} + k_f \left\{ \left[1 - \left(\frac{D}{D_o} \right)^2 \right] E_{d11} + \left(\frac{D}{D_o} \right)^2 E_{f11} \right\}$$

$$E_{\ell 22} = E_{m22} \left\{ \left(1 - \sqrt{k_f} \right) + \frac{\sqrt{k_f} \left(1 - \frac{D}{D_o} \right)}{1 - \sqrt{k_f} \left(1 - \frac{E_{m22}}{E_{d22}} \right)} + \frac{\sqrt{k_f} \left(\frac{D}{D_o} \right)}{1 - \sqrt{k_f} \left[1 - \left(1 - \frac{D}{D_o} \right) \frac{E_{m22}}{E_{d22}} - \left(\frac{D}{D_o} \right) \frac{E_{m22}}{E_{f22}} \right]} \right\} = E_{\ell 33}$$

$$G_{\ell 12} = G_{m12} \left\{ \left(1 - \sqrt{k_f} \right) + \frac{\sqrt{k_f} \left(1 - \frac{D}{D_o} \right)}{1 - \sqrt{k_f} \left(1 - \frac{G_{m12}}{G_{d12}} \right)} + \frac{\sqrt{k_f} \left(\frac{D}{D_o} \right)}{1 - \sqrt{k_f} \left[1 - \left(1 - \frac{D}{D_o} \right) \frac{G_{m12}}{G_{d12}} - \left(\frac{D}{D_o} \right) \frac{G_{m12}}{G_{f12}} \right]} \right\} = G_{\ell 13}$$

$$G_{\ell 23} = G_{m23} \left\{ \left(1 - \sqrt{k_f} \right) + \frac{\sqrt{k_f} \left(1 - \frac{D}{D_o} \right)}{1 - \sqrt{k_f} \left(1 - \frac{G_{m23}}{G_{d23}} \right)} + \frac{\sqrt{k_f} \left(\frac{D}{D_o} \right)}{1 - \sqrt{k_f} \left[1 - \left(1 - \frac{D}{D_o} \right) \frac{G_{m23}}{G_{d23}} - \left(\frac{D}{D_o} \right) \frac{G_{m23}}{G_{f23}} \right]} \right\}$$

$$\upsilon_{\ell 12} = k_m \upsilon_{m12} + k_f \left\{ \left[1 - \left(\frac{D}{D_o} \right)^2 \right] \upsilon_{d12} + \left(\frac{D}{D_o} \right)^2 \upsilon_{f12} \right\} = \upsilon_{\ell 13}$$

$$\upsilon_{\ell 23} = \frac{E_{\ell 22}}{2 G_{\ell 23}} - 1$$

Figure 6 – Composite Micromechanics Equations for Ply Mechanical Properties

uniaxial strengths are shown in Figures 7 and 8, respectively. In the equations: k denotes constituent volume fraction; D and D_o denote current and reference fiber diameters, respectively; E, G, and ν denote normal modulus, shear modulus, and Poisson's ratio, respectively; ρ, C, K, and α denote average density, average heat capacity, thermal conductivity, and coefficient of thermal expansion, respectively; S represents ultimate strength; β_{ft}, β_{fc}, and β_{cs} are empirical constants, and; the subscripts f, m, d, and ℓ denote an association to the fiber, matrix, interphase, and ply, respectively. The properties predicted by the equations in Figures 6 through 8 represent average values for an equivalent pseudo-homogeneous, transversely isotropic (isotropic in the 2-3 plane) ply.

In addition to predicting material properties for the unidirectional fiber-reinforced lamina, expressions were derived to predict the microstress distribution in the constituents resulting from the stress state occurring in the ply. This micromechanistic treatment of constituent stresses is illustrated in Figure 9. In the transverse direction (see Figure 5), the resulting components of microstress in the matrix and interphase (σ_{22}, σ_{12}, σ_{23}) are taken to be nonuniform through

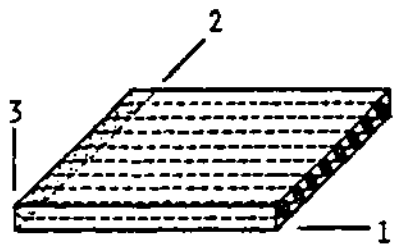

$$C_g = k_m\left(\frac{\rho_m}{\rho_g}\right)C_m + k_f\left\{\left[1-\left(\frac{D}{D_o}\right)^2\right]\left(\frac{\rho_d}{\rho_g}\right)C_d + \left(\frac{D}{D_o}\right)^2\left(\frac{\rho_f}{\rho_g}\right)C_f\right\}$$

$$K_{g11} = k_m K_{m11} + k_f\left\{\left[1-\left(\frac{D}{D_o}\right)^2\right]K_{d11} + \left(\frac{D}{D_o}\right)^2 K_{f11}\right\}$$

$$K_{g22} = K_{m22}\left\{\left(1-\sqrt{k_f}\right) + \frac{\sqrt{k_f}\left(1-\frac{D}{D_o}\right)}{1-\sqrt{k_f}\left(1-\frac{K_{m11}}{K_{d11}}\right)} + \frac{\sqrt{k_f}\left(\frac{D}{D_o}\right)}{1-\sqrt{k_f}\left[1-\left(1-\frac{D}{D_o}\right)\frac{K_{m11}}{K_{d11}}-\left(\frac{D}{D_o}\right)\frac{K_{m11}}{K_{f11}}\right]}\right\} = K_{g33}$$

$$\alpha_{g11} = k_m\left(\frac{E_{m11}}{E_{g11}}\right)\alpha_{m11} + k_f\left\{\left[1-\left(\frac{D}{D_o}\right)^2\right]\left(\frac{E_{d11}}{E_{g11}}\right)\alpha_{d11} + \left(\frac{D}{D_o}\right)^2\left(\frac{E_{f11}}{E_{g11}}\right)\alpha_{f11}\right\}$$

$$\alpha_{g22} = \frac{E_{m22}}{E_{g22}}\left\{\left(1-\sqrt{k_f}\right)\alpha_{m22} + \frac{\left(1-\frac{D}{D_o}\right)\left[\left(1-\sqrt{k_f}\right)\alpha_{m22} + \sqrt{k_f}\,\alpha_{d22}\right]}{1-\sqrt{k_f}\left(1-\frac{E_{m22}}{E_{d22}}\right)}\right.$$

$$\left. + \frac{\sqrt{k_f}\,C_{m22} - k_f\left[\alpha_{m22} - \left(1-\frac{D}{D_o}\right)\alpha_{d22} - \left(\frac{D}{D_o}\right)\alpha_{f22}\right]}{1-\sqrt{k_f}\left[1-\left(1-\frac{D}{D_o}\right)\frac{E_{m22}}{E_{d22}}-\left(\frac{D}{D_o}\right)\frac{E_{m22}}{E_{f22}}\right]}\right\} = \alpha_{g33}$$

Figure 7 - Composite Micromechanics Equations for Ply Thermal Properties

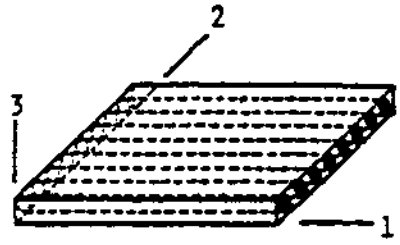

$$S_{\ell 11T} = S_{f11T}\left\{k_m\left(\frac{E_{m11}}{E_{f11}}\right) + \beta_{fT}\, k_f\left[\left(\frac{D}{D_o}\right)^2 + \left\{1 - \left(\frac{D}{D_o}\right)^2\right\}\frac{E_{d11}}{E_{f11}}\right]\right\}$$

$$S_{\ell 11C} = \text{MIN}\left\{\begin{array}{l} S_{f11C}\left\{k_m\left(\frac{E_{m11}}{E_{f11}}\right) + \beta_{fC}\, k_f\left[\left(\frac{D}{D_o}\right)^2 + \left\{1 - \left(\frac{D}{D_o}\right)^2\right\}\frac{E_{d11}}{E_{f11}}\right]\right\} \\ S_{m11C}\left\{k_m + \beta_{fC}\, k_f\left[\left(\frac{D}{D_o}\right)^2\frac{E_{f11}}{E_{m11}} + \left\{1 - \left(\frac{D}{D_o}\right)^2\right\}\frac{E_{d11}}{E_{m11}}\right]\right\} \\ G_{m12}\left\{\dfrac{1}{k_m + k_f\left[\left(\frac{D}{D_o}\right)^2\frac{G_{m12}}{G_{f12}} + \left\{1 - \left(\frac{D}{D_o}\right)^2\right\}\frac{G_{m12}}{G_{d12}}\right]}\right\} \\ S_{m11C} + \beta_{CS}\, S_{\ell 12} \end{array}\right.$$

Figure 8 - Composite Micromechanics Equations for Ply Uniaxial Strengths

$$S_{\ell 22T,\,C} = \frac{S_{m22T,\,C}}{\left\{1 - \sqrt{k_f}\left[1 - \left(1 - \frac{D}{D_o}\right)\frac{E_{m22}}{E_{d22}} - \left(\frac{D}{D_o}\right)\frac{E_{m22}}{E_{f22}}\right]\right\}\left[1 + \Phi(\Phi - 1) + 1/3(\Phi - 1)^2\right]^{1/2}}$$

WHERE;

$$\Phi = \frac{1}{\sqrt{\frac{\pi}{4k_f}} - 1}\left\{\sqrt{\frac{\pi}{4k_f}} - \frac{\left(\frac{E_{m22}}{E_{f22}}\right)}{1 - \sqrt{k_f}\left[1 - \left(1 - \frac{D}{D_o}\right)\frac{E_{m22}}{E_{d22}} - \left(\frac{D}{D_o}\right)\frac{E_{m22}}{E_{f22}}\right]}\right\}$$

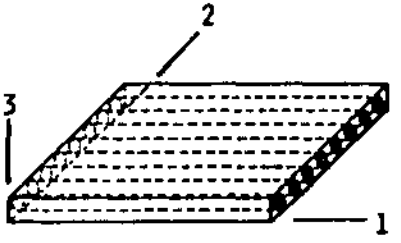

LOWER BOUND;

$$S_{\ell 22T,\,C} = \left(1 - \sqrt{\frac{4k_f}{\pi}}\right)S_{m22T,\,C}$$

EQUATIONS FOR INTRALAMINAR SHEAR STRENGTH ($S_{\ell 12}$) ARE ANALOGOUS TO ABOVE EQUATIONS WITH E AND $S_{m22T,\,C}$ REPLACED BY G AND S_{m12}, RESPECTIVELY

Figure 8 - cont'd

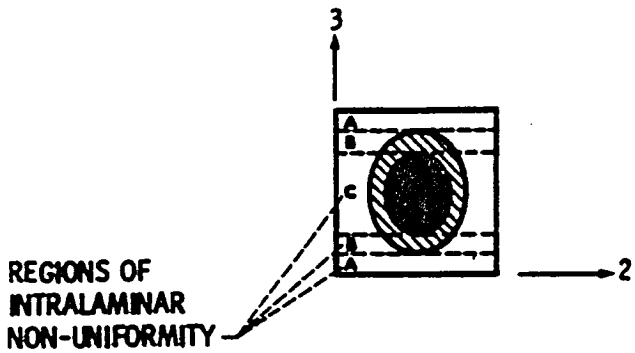

AVERAGE CONSTITUENT PROPERTIES;

$$E_{m22} = \frac{1}{1+\sqrt{k_f}}\left[E_{m22}^{(A)} + \left(1-\frac{D}{D_0}\right)E_{m22}^{(B)} + \sqrt{k_f}\left(\frac{D}{D_0}\right)E_{m22}^{(C)}\right]$$

EQUATIONS FOR G_{m12}, G_{m23}, K_{m22}, AND α_{m22} ARE ANALOGOUS TO EQUATION FOR E_{m22}

$$E_{d22} = \frac{1}{1+\left(\frac{D}{D_0}\right)}\left[E_{d22}^{(B)} + \left(\frac{D}{D_0}\right)E_{d22}^{(C)}\right]$$

EQUATIONS FOR G_{d12}, G_{d23}, K_{d22}, AND α_{d22} ARE ANALOGOUS TO EQUATION FOR E_{d22}

Figure 9 - Regions of Intralaminar Nonuniformity for Constituent Transverse Microstresses and Properties

the ply thickness. By virtue of the formulation of the nonlinear TVP relationships discussed earlier, this nonuniformity of transverse microstresses results in a nonuniformity of transverse material properties (mechanical and thermal) for the matrix and interphase. The schematic in Figure 9 shows the model used to distinguish different regions or zones of intralaminar nonuniformity for matrix and interphase transverse microstresses and material properties. Also in Figure 9 are equations for calculating the "average" matrix and interphase transverse properties which are used in the composite micromechanics equations used to predict transverse properties for the unidirectional lamina. The distribution of microstresses in the constituents resulting from the stress state occurring in a lamina are predicted from the composite micromechanics equations shown in Figure 10. In the equations of Figures 9 and 10: the superscripts A, B, and C denote the regions or zones of intralaminar nonuniformity; σ denotes stress; ΔT denotes temperature increment, and; all other quantities are as defined earlier.

In one sense, the composite micromechanics equations presented here can be thought of as a first level of approximation for idealizing a laminated TFRS composite HPT blade/vane component as a pseudo-homogeneous

$$\sigma_{f11} = \left[\frac{\sigma_{\ell 11}}{E_{\ell 11}} + \Delta T\,(\alpha_{\ell 11} - \alpha_{f11})\right] E_{f11}$$

$$\sigma_{f22} = \frac{E_{f22}\left\{\frac{\sigma_{\ell 22}}{E_{\ell 22}} + \Delta T\left[\alpha_{\ell 22} - (1-\sqrt{k_f})\,\alpha_{m22}^{(C)} - \sqrt{k_f}\left(1-\frac{D}{D_o}\right)\alpha_{d22}^{(C)} - \sqrt{k_f}\left(\frac{D}{D_o}\right)\alpha_{f22}\right]\right\}}{1-\sqrt{k_f}\left[1-\left(1-\frac{D}{D_o}\right)\frac{E_{m22}}{E_{d22}} - \left(\frac{D}{D_o}\right)\frac{E_{m22}}{E_{f22}}\right]}$$

$$\sigma_{f12} = \frac{\left(\frac{\sigma_{\ell 12}}{G_{\ell 12}}\right) G_{f12}}{1-\sqrt{k_f}\left[1-\left(1-\frac{D}{D_o}\right)\frac{G_{m12}}{G_{d12}} - \left(\frac{D}{D_o}\right)\frac{G_{m12}}{G_{f12}}\right]}$$

EQUATION FOR σ_{f23} IS ANALOGOUS TO EQUATION FOR σ_{f12}

Figure 10 - Composite Micromechanics Equations for Constituent Microstresses

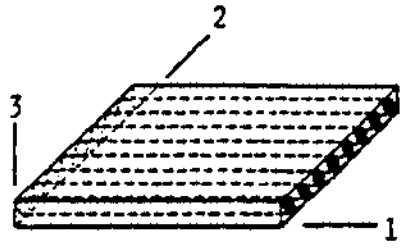

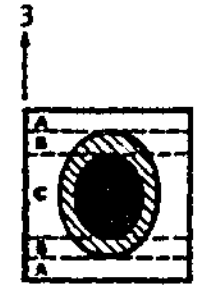

$$\sigma_{m11} = \left[\frac{\sigma_{f11}}{E_{f11}} + \Delta T\,(\alpha_{f11} - \alpha_{m11})\right] E_{m11}$$

$$\sigma_{m22}^{(A)} = \left[\frac{\sigma_{f22}}{E_{f22}} + \Delta T\left(\alpha_{f22} - \alpha_{m22}^{(A)}\right)\right] E_{m22}^{(A)}$$

$$\sigma_{m22}^{(B)} = \frac{E_{m22}^{(B)}\left\{\frac{\sigma_{f22}}{E_{f22}} + \Delta T\left[\alpha_{f22} - (1-\sqrt{k_f})\,\alpha_{m22}^{(B)} - \sqrt{k_f}\,\alpha_{d22}^{(B)}\right]\right\}}{1-\sqrt{k_f}\left(1-\frac{E_{m22}}{E_{d22}}\right)}$$

$$\sigma_{m22}^{(C)} = \frac{E_{m22}^{(C)}\left\{\frac{\sigma_{f22}}{E_{f22}} + \Delta T\left[\alpha_{f22} - (1-\sqrt{k_f})\,\alpha_{m22}^{(C)} - \sqrt{k_f}\left(1-\frac{D}{D_o}\right)\alpha_{d22}^{(C)} - \sqrt{k_f}\left(\frac{D}{D_o}\right)\alpha_{f22}\right]\right\}}{1-\sqrt{k_f}\left[1-\left(1-\frac{D}{D_o}\right)\frac{E_{m22}}{E_{d22}} - \left(\frac{D}{D_o}\right)\frac{E_{m22}}{E_{f22}}\right]}$$

$$\sigma_{m12}^{(A)} = \left(\frac{\sigma_{f12}}{G_{f12}}\right) G_{m12}^{(A)}$$

$$\sigma_{m12}^{(B)} = \frac{\left(\frac{\sigma_{f12}}{G_{f12}}\right) G_{m12}^{(B)}}{1-\sqrt{k_f}\left(1-\frac{G_{m12}}{G_{d12}}\right)}$$

$$\sigma_{m12}^{(C)} = \frac{\left(\frac{\sigma_{f12}}{G_{f12}}\right) G_{m12}^{(C)}}{1-\sqrt{k_f}\left[1-\left(1-\frac{D}{D_o}\right)\frac{G_{m12}}{G_{d12}} - \left(\frac{D}{D_o}\right)\frac{G_{m12}}{G_{f12}}\right]}$$

EQUATIONS FOR $\sigma_{m23}^{(A,\,B,\,C)}$ ARE ANALOGOUS TO EQUATIONS FOR $\sigma_{m12}^{(A,\,B,\,C)}$

Figure 10 - cont'd

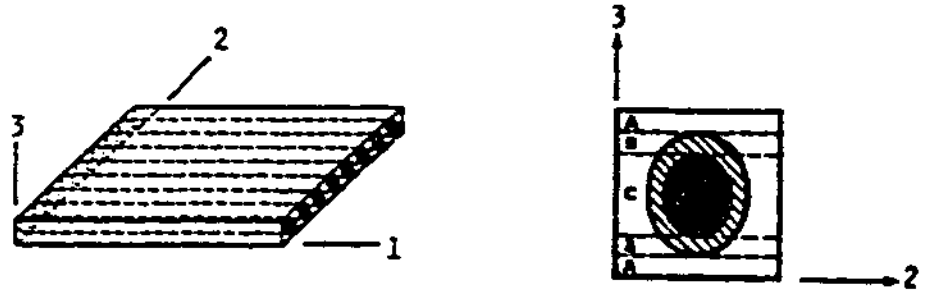

$$\sigma_{d11} = \left[\frac{\sigma_{f11}}{E_{f11}} + \Delta T\,(\alpha_{f11} - \alpha_{d11})\right] E_{d11}$$

$$\sigma_{d22}^{(B)} = \frac{E_{d22}^{(B)}\left\{\frac{\sigma_{f22}}{E_{f22}} + \Delta T\left[\alpha_{f22} - \alpha_{d} - \sqrt{v_f}\,\alpha_{m22}^{(B)} - \sqrt{v_f}\,\alpha_{d22}^{(B)}\right]\right\}}{1 - \sqrt{v_f}\left(1 - \frac{E_{m22}}{E_{d22}}\right)}$$

$$\sigma_{d22}^{(C)} = \frac{E_{d22}^{(C)}\left\{\frac{\sigma_{f22}}{E_{f22}} + \Delta T\left[\alpha_{f22} - \alpha_{d} - \sqrt{v_f}\,\alpha_{m22}^{(C)} - \sqrt{v_f}\left(1 - \frac{D}{D_0}\right)\alpha_{d22}^{(C)} - \sqrt{v_f}\left(\frac{D}{D_0}\right)\alpha_{f22}\right]\right\}}{1 - \sqrt{v_f}\left[1 - \left(1 - \frac{D}{D_0}\right)\frac{E_{m22}}{E_{d22}} - \left(\frac{D}{D_0}\right)\frac{E_{m22}}{E_{f22}}\right]}$$

$$\sigma_{d12}^{(B)} = \frac{\left(\frac{\sigma_{f12}}{G_{f12}}\right)G_{d12}^{(B)}}{1 - \sqrt{v_f}\left(1 - \frac{G_{m12}}{G_{d12}}\right)}$$

$$\sigma_{d12}^{(C)} = \frac{\left(\frac{\sigma_{f12}}{G_{f12}}\right)G_{d12}^{(C)}}{1 - \sqrt{v_f}\left[1 - \left(1 - \frac{D}{D_0}\right)\frac{G_{m12}}{G_{d12}} - \left(\frac{D}{D_0}\right)\frac{G_{m12}}{G_{f12}}\right]}$$

EQUATIONS FOR $\sigma_{d23}^{(B,\,C)}$ ARE ANALOGOUS TO EQUATIONS FOR $\sigma_{d12}^{(B,\,C)}$

Figure 10 - cont'd

structure. In order to obtain an indication of the accuracy and validity of the composite micromechanics equations, a finite element study was conducted to compare the predictions of average mechanical and thermal properties from the micromechanics equations with the average property values simulated in a finite element structural analysis. A brief discussion of the details and results of the finite element study is given in the appendix. In general, the values for properties as predicted by the composite micromechanics equations were found to be in excellent agreement with the values obtained by the finite element analysis.

2.3.4 Laminate Theory

In short, laminate theory (laminated plate theory) provides the formal structure to relate the behavior of a laminated composite structure to the behavior of the individual laminate of the composite. As discussed in the previous section, a unidirectional fiber-reinforced lamina can be approximated as a homogeneous orthotropic ply. From assumptions analogous to the Kirchhoff hypotheses in classical homogeneous plate theory (see ref. 16) the laminae of a laminated composite structure are treated as thin plates and therefore are assumed to exist in a plane stress state. As such, the constitutive relationship for

the k^{th} specially orthotropic ply (referred to the lamina material coordinate system) is given by (see ref. 9);

$$\begin{Bmatrix} \varepsilon_{11} \\ \varepsilon_{22} \\ \varepsilon_{12} \end{Bmatrix}_k = \begin{bmatrix} E_{11} & E_{12} & 0 \\ E_{12} & E_{22} & 0 \\ 0 & 0 & E_{66} \end{bmatrix}_k^{-1} \begin{Bmatrix} \sigma_{11} \\ \sigma_{22} \\ \sigma_{12} \end{Bmatrix}_k \tag{1}$$

In terms of stress, equation (1) can be rewritten in condensed form as;

$$\{\sigma_{\ell m}\}_k = [E_{\ell m}]_k \{\varepsilon_{\ell m}\}_k \tag{2}$$

where the subscript m indicates ply material coordinate system. For the generally orthotropic ply (referred to

the global structural coordinate system) the constitutive relationship is given by;

$$\{\sigma_{\ell s}\}_k = \begin{Bmatrix} \sigma_{xx} \\ \sigma_{yy} \\ \sigma_{xy} \end{Bmatrix}_k = [R_{\ell\varepsilon}]_k^T \, [E_{\ell m}]_k \, [R_{\ell\varepsilon}]_k \begin{Bmatrix} \varepsilon_{xx} \\ \varepsilon_{yy} \\ \varepsilon_{xy} \end{Bmatrix}_k \qquad (3)$$

$$= [E_{\ell s}]_k \, \{\varepsilon_{\ell s}\}_k$$

where the subscript s indicates global structural coordinate system. The matrix $[R_{\ell\varepsilon}]$ is the rotation or transformation matrix and is defined as;

$$[R_{\ell\varepsilon}]_k = \begin{bmatrix} \cos^2\theta & \sin^2\theta & \tfrac{1}{2}\sin 2\theta \\ \sin^2\theta & \cos^2\theta & -\tfrac{1}{2}\sin 2\theta \\ -\sin 2\theta & \sin 2\theta & \cos 2\theta \end{bmatrix}_k \qquad (4)$$

and the angle θ represents the orientation of the lamina material coordinate axes (1,2) for the k^{th} ply with respect to the global structural coordinate axes (x,y).

For the linear case, it can be shown (see ref. 16) that the strain in any ply is related to the strain of the geometric midplane of the laminate (ε^o_{xx}, ε^o_{yy}, ε^o_{xy}) and the curvature of the laminate (κ_{xx}, κ_{yy}, κ_{xy}). In terms of the midplane strain and laminate curvature, the constitutive relationship for the k^{th} generally orthotropic lamina becomes;

$$\{\sigma_{\ell s}\}_k = [E_{\ell s}]_k \{\varepsilon_{\ell s}\}_k = [E_{\ell s}]_k (\{\varepsilon^0_c\} + z^0_\ell \{\kappa_c\}) \quad (5)$$

where the subscript c denotes composite or laminate and z^o_ℓ is the perpendicular distance from the laminate midplane to the center of the k^{th} ply.

In general, the stresses from ply to ply in a laminate will vary. However, it is possible to resolve the stresses in all of the plies of an infinitesimal parallelopiped element of a laminate into an equivalent system of stress and moment resultants which are taken to act at the geometric midplane of the laminate (see Figure 11). The stress resultants (N_x, N_y, N_{xy}) and moment resultants (M_x, M_y, M_{xy}) are given by the following equations (see ref. 16);

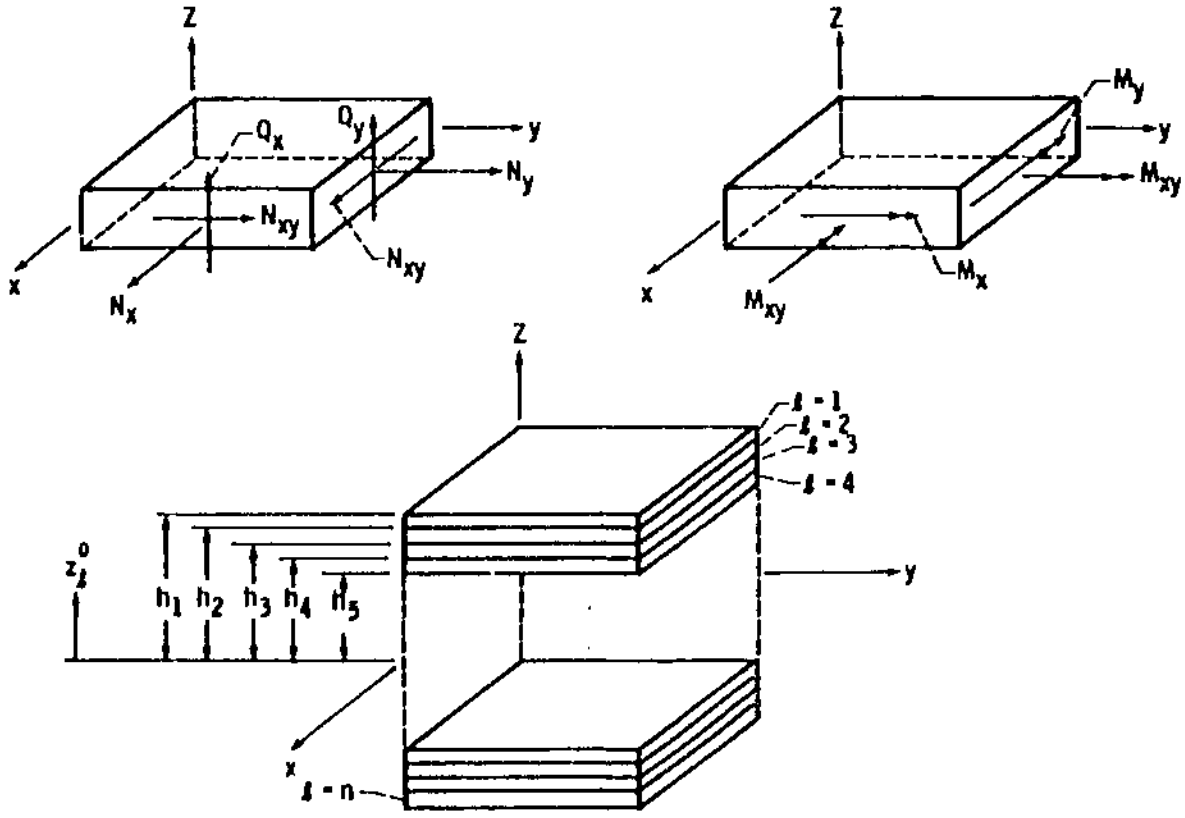

Figure 11 - Definition of Laminate Midplane Stress and Moment Resultants and Structural Coordinate System

$$\{N_c\} = \begin{Bmatrix} N_x \\ N_y \\ N_{xy} \end{Bmatrix} = \int_{-h/2}^{h/2} \begin{Bmatrix} \sigma_{xx} \\ \sigma_{yy} \\ \sigma_{xy} \end{Bmatrix} dz \qquad (6a)$$

$$\{M_c\} = \begin{Bmatrix} M_x \\ M_y \\ M_{xy} \end{Bmatrix} = \int_{-h/2}^{h/2} \begin{Bmatrix} \sigma_{xx} \\ \sigma_{yy} \\ \sigma_{xy} \end{Bmatrix} z\,dz \qquad (6b)$$

The single continuous integrals in equations (6) can be separated into sums of simple integrals over each ply (see Figure 11). As such, the stress and moment resultants are given by;

$$\{N_c\} = \sum_{k=1}^{n} \int_{h_{k-1}}^{h_k} \{\sigma_{\ell s}\}_k \, dz \tag{7a}$$

$$\{M_c\} = \sum_{k=1}^{n} \int_{h_{k-1}}^{h_k} \{\sigma_{\ell s}\}_k \, z \, dz \tag{7b}$$

Substituting the stress as given in equation (5) into equations (7) above and bringing the constant terms outside the integral yields;

$$\{N_c\} = \sum_{k=1}^{n} \left([E_{\ell s}]_k \{\varepsilon_c^0\} \int_{h_{k-1}}^{h_k} dz + [E_{\ell s}]_k \{\kappa_c\} \int_{h_{k-1}}^{h_k} z \, dz \right) \tag{8a}$$

$$\{M_c\} = \sum_{k=1}^{n} \left([E_{\ell s}]_k \{\varepsilon_c^0\} \int_{h_{k-1}}^{h_k} z \, dz + [E_{\ell s}]_k \{\kappa_c\} \int_{h_{k-1}}^{h_k} z^2 \, dz \right) \tag{8b}$$

Evaluation and simplification of the integrals in equations (8) gives;

$$\{N_c\} = [A_c]\ \{\varepsilon_c^0\} + [C_c]\ \{\kappa_c\} \tag{9a}$$

$$\{M_c\} = [C_c]\ \{\varepsilon_c^0\} + [D_c]\ \{\kappa_c\} \tag{9b}$$

where,

$$[A_c] = \sum_{k=1}^{n} [E_{ls}]_k\ (z_k - z_{k-1}) \tag{10a}$$

$$[C_c] = \frac{1}{2} \sum_{k=1}^{n} [E_{ls}]_k\ (z_k^2 - z_{k-1}^2) \tag{10b}$$

$$[D_c] = \frac{1}{3} \sum_{k=1}^{n} [E_{ls}]_k\ (z_k^3 - z_{k-1}^3) \tag{10c}$$

Equations (9) are usually referred to as the constitutive relationship for the laminate whereas equations (10) define the laminate membrane, bending, and coupled membrane-bending stiffnesses, respectively.

Although the through-the-thickness stresses (σ_{33}, σ_{23}, σ_{13}) are neglected in deriving the constitutive relationships for the orthotropic lamina, these stresses generally will exist in the laminate. These stresses are typically determined from equilibrium considerations. From the concept of moment equilibrium for an elemental parallelopiped of a laminate, it can be shown (see ref. 16) that the through-the-thickness shear stress resultants for the laminate are given by (see Figure 11);

$$Q_x = \frac{\partial M_x}{\partial x} + \frac{\partial M_{xy}}{\partial y} \tag{11a}$$

$$Q_y = \frac{\partial M_{xy}}{\partial x} + \frac{\partial M_y}{\partial y} \tag{11b}$$

Similarly, by applying the concept of force equilibrium for the elemental parallelopiped of a laminate, the

through-the-thickness normal stress can be determined from the following equation;

$$\frac{\partial \sigma_z}{\partial z} = \frac{\partial \sigma_{xz}}{\partial x} + \frac{\partial \sigma_{yz}}{\partial y} \tag{12}$$

Assuming a parabolic distribution of shear stress (σ_{xy}, σ_{yz}) over the plate thickness (which constitutes a rectangular cross-section), the through-the-thickness shear stresses for the ply are given by;

$$\sigma_{\ell xz} = \frac{3}{4} \frac{Q_x}{h} \left[1 - \left(\frac{z^0_\ell}{h}\right)^2\right] \tag{13a}$$

$$\sigma_{\ell yz} = \frac{3}{4} \frac{Q_y}{h} \left[1 - \left(\frac{z^0_\ell}{h}\right)^2\right] \tag{13b}$$

The through-the-thickness normal stress for the ply is found by substituting equations (13) into equation (12) and integrating, which yields;

$$\sigma_{\ell zz} = \left(\frac{\partial Q_x}{\partial x} + \frac{\partial Q_y}{\partial y}\right) \left\{\frac{3}{4}\left[\frac{z^0_\ell}{h} - \frac{1}{3}\left(\frac{z^0_\ell}{h}\right)^3\right]\right\} \tag{14}$$

A summary of the governing equations of laminate theory is given in Figure 12. The contributions of thermal loading are included in these equations. In these equations the subscript c denotes laminate and all other quantities are as defined earlier.

The cursory discussion of laminate theory here was presented only for completeness in summarizing the key elements comprising the upward-integrated top-down-structured approach to nonlinear structural analysis taken here. For a more thorough treatment of this subject, the reader is directed to one of the references cited earlier in this section.

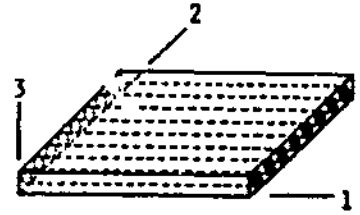

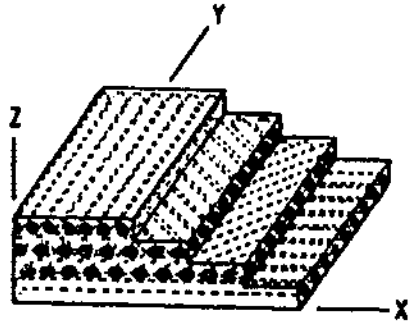

PLY CONSTITUTIVE RELATIONSHIP: $(\epsilon)_\ell = [E]_\ell^{-1} (\sigma)_\ell + \Delta T_\ell (\alpha)_\ell$

PLY STRAIN: $(\epsilon)_\ell = [R_\epsilon]_\ell \left\langle (\epsilon^0)_C - Z_\ell^0 (\kappa)_C \right\rangle$

PLY STRESS: $(\sigma)_\ell = [E]_\ell \left\langle (\epsilon)_\ell - \Delta T_\ell (\alpha)_\ell \right\rangle$

LAMINATE CONSTITUTIVE RELATIONSHIP: $\left\{ \begin{matrix} N \\ M \end{matrix} \right\}_C = \left[\begin{array}{c|c} A & C \\ \hline C^T & D \end{array} \right]_C \left\{ \begin{matrix} \epsilon^0 \\ \kappa \end{matrix} \right\}_C - \left\{ \begin{matrix} N_T \\ M_T \end{matrix} \right\}_C$

LAMINATE THERMAL FORCES/MOMENTS: $(N_T, M_T)_C = \sum_{\ell=1}^{n} [R_\epsilon]_\ell^T [E]_\ell (\alpha)_\ell \Delta T_\ell \left\langle (h_\ell - h_{\ell-1}), 1/2(h_\ell^2 - h_{\ell-1}^2) \right\rangle$

LAMINATE STIFFNESS: $[A, C, D]_C = \sum_{\ell=1}^{n} [R_\epsilon]_\ell^T [E]_\ell [R_\epsilon]_\ell \left\langle (h_\ell - h_{\ell-1}), 1/2(h_\ell^2 - h_{\ell-1}^2), 1/3(h_\ell^3 - h_{\ell-1}^3) \right\rangle$

Figure 12 - Summary of Governing Equations of Laminate Theory

CHAPTER 3

COMPUTER IMPLEMENTATION

3.1 Introduction

In Chapter 2 the theoretical aspects concerned with the nonlinear analysis of a composite structure were discussed. In addition, an upward-integrated top-down-structured approach was presented for the nonlinear structural analysis of TFRS composite engine HPT blade/vane components. Attention here is turned to the issue of computer programming effort required to implement this upward-intergrated top-down-structured approach into a computerized structural analysis tool.

To develop the analytical capability alluded to above, the COBSTRAN structural analysis software package was used as a foundation, as mentioned in Chapter 1. Generally speaking, efforts toward the development of a nonlinear version of COBSTRAN involved: implementation of new computer program modules into COBSTRAN to incorporate the fiber degradation model, nonlinear TVP material model, and modified composite micromechanics equations into the analytical solution process; implementation of new

computer program modules for input/output; modification of existing COBSTRAN modules to provide additional capabilities; expansion and restructuring of the execucive module in COBSTRAN; and development of a job control command structure to support the incremental/iterative solution strategy imbedded in the upward-integrated top-down-structured approach on which nonlinear COBSTRAN is based. In total, the programming efforts involved in the development of nonlinear COBSTRAN amounted to approximately 3000 additional lines of FORTRAN code and 400 lines of job control commands. A categorized summary of the most significant of these efforts is provided here, following an overview of the original COBSTRAN package.

3.2 COBSTRAN Overview

As described in Chapter 1, COBSTRAN is a software package which was developed at the NASA Lewis Research Center as an in-house research and development tool for performing linear-elastic structural analysis of composite blade structures. In short, the package is comprised of: the COBSTRAN code which is a modular FORTRAN program functioning as a preprocessor and postprocessor for general purpose finite element structural analysis codes, and; the job control command structure which provides the necessary data file management and provides the interface to link the COBSTRAN program and the finite element code.

At the Lewis Research Center, COBSTRAN is used in conjunction with the MSC/NASTRAN (ref. 17) general purpose finite element code on an IBM 370/CRAY 1S computer network.

COBSTRAN is designed to analyze two basic types of blade structures. The first type encompasses a solid blade geometry with the option for including hollow core cavities or inlays. The second type encompasses a hollow-shell blade geometry with the option for including interior spar-like stiffeners. The solid geometry would be typical of a solid turbine blade/vane while the hollow-shell geometry would be typical of a wind turbine blade or other wing-like structure.

As a preprocessor for MSC/NASTRAN, the capabilities of the COBSTRAN code include: interpolation of the blade geometry in the spanwise, chordwise and thickness directions; determination of the ply lay-up for the composite blade model; interpolation of the blade temperature and pressure distributions; generation of the discretized finite element mesh for the blade model (at present COBSTRAN supports triangular and quadrilateral plate elements); determination of the element material properties using the appropriate composite micromechanics theory and laminate theory; and generation of the MSC/NASTRAN bulk data input deck.

As a postprocessor for MSC/NASTRAN, the capabilities of COBSTRAN include: processing of element stress results from the finite element analysis, and; determination of individual ply stresses/strains, interply stresses, and ply failure margins of safety using the appropriate laminate theory, composite micromechanics theory and combined-stress strength failure criteria.

3.3 Development of Nonlinear COBSTRAN

3.3.1 Fiber Degradation Model

As discussed in Chapter 2, the fiber degradation phenomenon can have a significant affect on the structural integrity of certain TFRS composite fiber/matrix systems such that accountability of the phenomenon in a structural analysis is warranted. In order to incorporate the fiber degradation phenomenon into the analytical solution process of nonlinear COBSTRAN, a computer program module (SUBROUTINE DEGRAD) was developed to implement the empirical expression presented in Chapter 2 (see Figure 3). The function of SUBROUTINE DEGRAD is to quantify the extent of fiber degradation occurring in the ply in terms of the incremental penetration (R) of the reaction zone or interphase. The incremental interphase penetration is used to determine the cumulative degradation and the ratio of current fiber diameter to reference fiber diameter

(D/D_o) for each ply at each node of the discretized blade model. In applying the fiber degradation equation, the exposure temperature is taken to be the average temperature for the particular load/time increment.

3.3.2 Nonlinear TVP Material Relationships

It was mentioned earlier that the nonlinear behavior of a TFRS composite is assumed to be attributable to a stress-temperature-time dependency of the constituent material properties. Nonlinear TVP relationships were presented (see Figure 4) to model the constituent material nonlinearity in a structural analysis. Individual computer program modules (SUBROUTINE, E, CP, K, ALPHA, and S) were developed to implement the nonlinear TVP relationships into the solution process of nonlinear COBSTRAN. In applying the nonlinear TVP relationships, the variables appearing in the expressions are taken as positive in sign. The appropriate component of the tensor variables (σ and S) is that which corresponds to the direction associated with the material property in question. For example, σ_{11}, $\dot{\sigma}_{11}$, and S_{11} are the appropriate components of stress, stress rate and ultimate strength for modifying the longitudinal normal modulus E_{11}. For the case of a material having different values of ultimate strength in tension and compression, the

appropriate value is determined according to the sense of the corresponding stress component (i.e., tensile or compressive).

The function of the material model computer program modules is to update the constituent material properties (E, C_p, K, α and S) at each iteration in the incremental/iterative solution process. The material property modification is performed for the constituents of each ply at each node of the discretized blade model.

3.3.3 Composite Micromechanics Equations

The composite micromechanics theory discussed in Chapter 2 provides the basis for idealizing a unidirectional fiber-reinforced composite lamina as an equivalent pseudo-homogeneous thin plate. Composite micromechanics equations were presented (see Figures 6-8) for predicting average material properties of the ply from the corresponding properties of the constituents of the ply. Computer modules (SUBROUTINE YOUNG, GMODS, POISS, HEAT, CONDUC, THERMX, and STREN) were developed to implement the equations into the solution process of nonlinear COBSTRAN. The function of the composite micromechanics computer program modules is to predict the current values of material properties for each ply at each node of the discretized blade model.

In addition to the equations for predicting ply material properties, composite micromechanics equations were presented in Chapter 2 (see Figure 10) to predict the distribution of microstresses in the constituents resulting from the stress state occurring in the ply. A computer program module (SUBROUTINE SIGMA) was developed to implement the equations into the solution process of nonlinear COBSTRAN. The function of the module is to compute the current constituent microstress distribution for each ply at each node of the discretized blade model.

3.3.4 Material Failure Theory

In connection with the discussion here on constituent microstresses, it seems appropriate at this point to address the subject of constituent material failure. Currently, nonlinear COBSTRAN utilizes what may be characterized as a "maximum-stress" failure criterion to predict "failure" in the constituents of a composite lamina. The criterion is based on the premise that the constituent material will support a magnitude of stress not greater than the corresponding strength available in the material. In the incremental/iterative solution strategy of nonlinear COBSTRAN, the failure criterion is imposed at each iteration. If, at a particular iteration

during the solution process, a computed microstress for a constituent material exceeds the currently available strength of the constituent, the material is assumed to have failed and the stiffness (modulus) of the constituent is defaulted to zero. As the solution process proceeds with the next equilibrium-convergence iteration, the stress state (micro and macro) in the vicinity of the simulated failure is, in effect, redistributed.

3.3.5 Geometry Updating

As described earlier, the solution strategy of the upward-integrated top-down-structured approach on which nonlinear COBSTRAN is based involves the incremental/iterative application of a linear problem formulation. In approaching the problem in this manner, it is possible to update the geometrical (as well as the material) aspects of the problem formulation from increment to increment during the solution process. In view of this, the capabilities of nonlinear COBSTRAN were expanded to include postprocessing of the discretized finite element mesh nodal coordinates using the nodal displacement results from the finite element analysis. The model geometry update is performed upon convergence of the solution for each load/time increment.

3.3.6 Convergence Criterion

In Chapter 2 it was mentioned that the incremental/iterative solution strategy imbedded in the upward-integrated top-down-structured approach for nonlinear composite structural analysis involves two levels of iteration during the solution process. The primary level of iteration occurs for the load/time increments. The secondary level of iteration occurs for each separate load/time increment and serves as an equilibrium-solution convergence iteration. The criterion to establish whether or not the analysis for a particular load/time increment has converged at an equilibrium solution involves the errors for nodal displacements between two consecutive iterations and is expressed as;

$$\frac{u_{i+1} - u_i}{u_{i+1}} \leq \text{tolerance} \qquad (15)$$

where u_i and u_{i+1} are the components of the nodal displacement vectors resulting from the finite element analysis for the two consecutive iterations. The tolerance against which the nodal displacement errors are compared is a prescribed quantity.

3.4 General Flowchart

An informal flowchart for the nonlinear COBSTRAN structural analysis package is shown in Figure 13. This flowchart is intended only to give the functional essence of nonlinear COBSTRAN by illustrating its operation at the most general level.

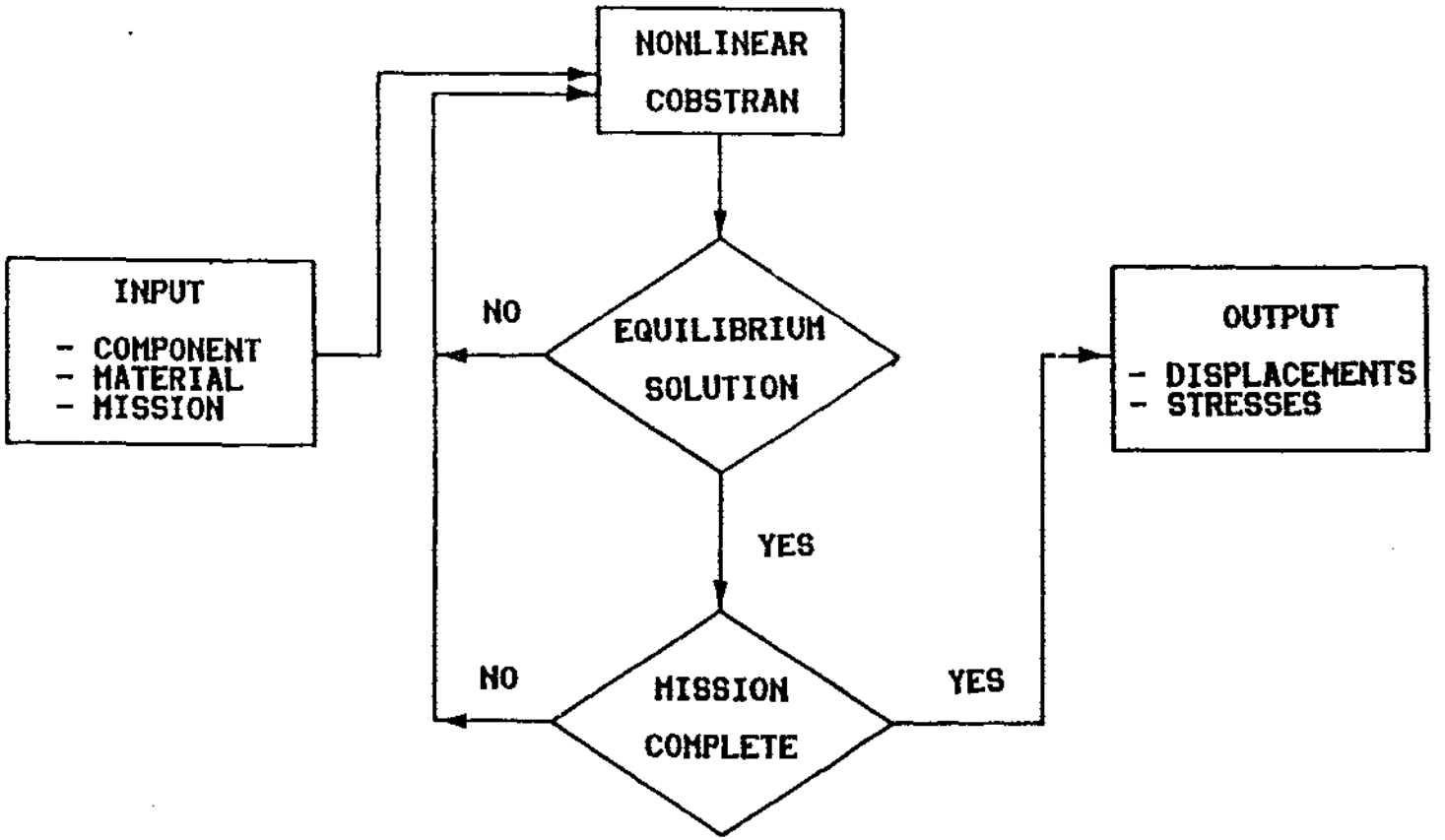

Figure 13 - General Flowchart of Nonlinear COBSTRAN Analysis Package

CHAPTER 4

DEMONSTRATION PROBLEM

4.1 Introduction

The discussion in Chapter 3 focused on the major programming efforts involved in implementing the upward-integrated top-down-structured approach for composite structural analysis into a computerized capability (nonlinear COBSTRAN) specifically tailored for the nonlinear analysis of TFRS composite turbine blade/vane components. The intent in this chapter is to manifest the general utility of the upward-integrated top-down-structured approach and to demonstrate the current capability represented by the nonlinear COBSTRAN structural analysis package. For this purpose, a demonstration problem is presented here in which nonlinear COBSTRAN was used to analyze an hypothetical TFRS composite HPT blade for a simulated fabrication process and a simulated engine mission. Analysis for the fabrication process was conducted to investigate the residual stresses induced in the airfoil. Analysis for the engine mission was conducted to investigate the overall response of the blade.

Before proceeding with the discussion of the demonstration problem, certain points made earlier should be re-stated. As mentioned in Chapter 1, the development of nonlinear COBSTRAN was undertaken as an evolutionary task. The emphasis in developing this structural analysis capability specifically tailored for TFRS composite turbine blades/vanes was to account for the governing physical phenomena affecting this application in the analytical formulation of the problem. To what extent this has been accomplished remains to be evaluated. At this point in time, nonlinear COBSTRAN must be considered strictly as a developmental research tool. As such, the results presented for this demonstration problem should be taken in proper perspective, i.e., as preliminary results only.

In view of the discussion above, this demonstration problem is not presented as an attempt to provide a user's guide to the operation of the nonlinear COBSTRAN package. Therefore, rather than dwell on the details involved in conducting an analysis, the emphasis here is on highlighting the types of information provided by an analysis using nonlinear COBSTRAN. In addition to the information pertaining to global structural response, nonlinear COBSTRAN provides more local information related to the change in state (in terms of material properties

and field variables) of each ply and its constituents at each node on a discretized blade structure.

4.2 TFRS Turbine Blade Component

As mentioned above, the demonstration problem presented here concerns analyses of an hypothetical TFRS composite HPT blade, or more specifically the airfoil portion of the blade, for a simulated fabrication process and a simulated engine mission. In general, the airfoil was of the hollow-shell type with no interior spars or stiffeners. With minor exceptions, the geometrical characteristics for this airfoil were typical of the airfoil characteristics of contemporary turbine blades currently in use in aircraft engines.

The airfoil geometry was defined in a rectangular (x, y, z) coordinate system such that the y-coordinate axis represented the axis-of-rotation of the airfoil and, assuming the airfoil to be untilted, the x-coordinate axis represented the stacking-axis of the airfoil. Definition of the airfoil geometry in this rectangular coordinate system is illustrated in Figure 14(a) which shows the discretized finite element model generated by nonlinear COBSTRAN for this demonstration problem. The model was comprised of 240 nodes and 220 quadrilateral isoparametric membrane-bending elements (MSC/NASTRAN CQUAD4 type).

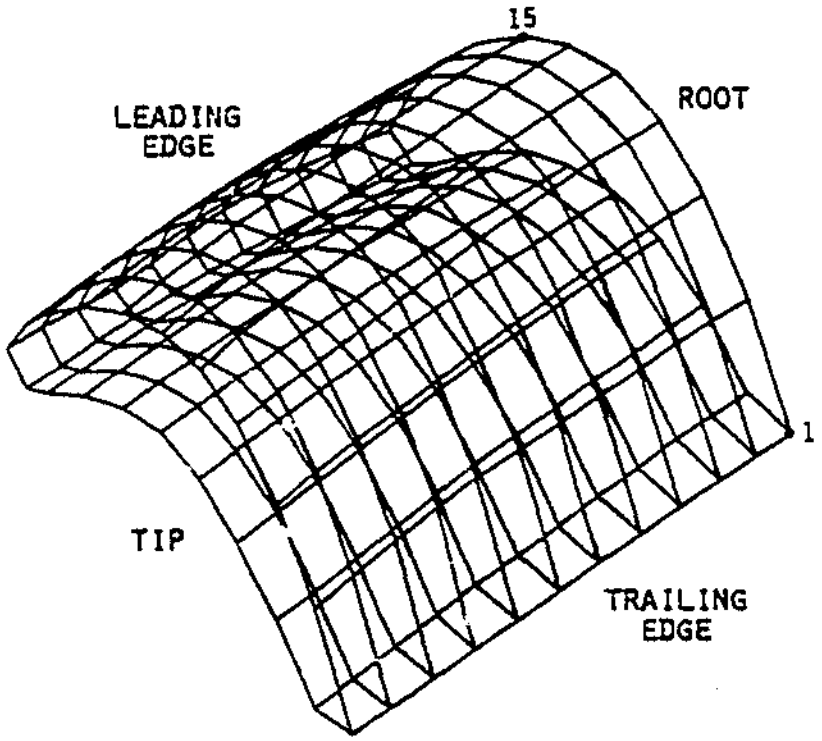

(a) Finite Element Mesh

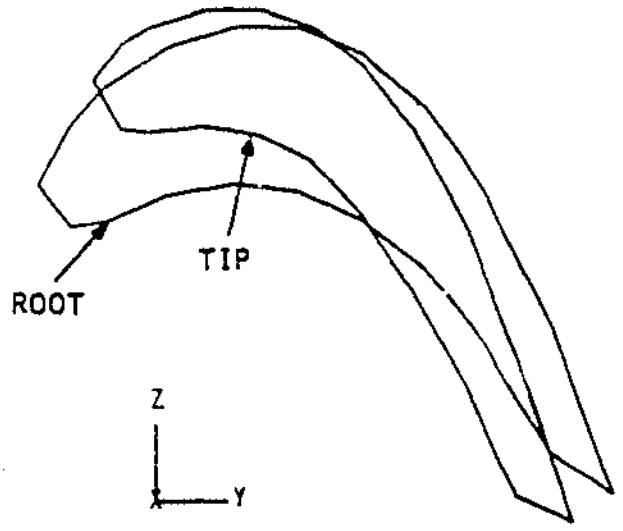

(b) Axial View of Root and Tip Cross-sections

Figure 14 - HPT Blade Airfoil Model

The root cross-section of the airfoil was assumed to be parallel to the yz-coordinate plane and located approximately 16.54 in. from the axis-of-rotation. The length (spanwise dimension) of the airfoil was approximately 2.15 in. from root cross-section to tip cross-section. The width (chordwise dimension) of the airfoil was approximately 1.20 in. and constant from root to tip, however, the cross-sectional area enclosed by the airfoil tapered from root to tip. Furthermore, the airfoil was twisted such that the angle-of-attack increased approximately 14^{o} from root to tip. The taper and twist characteristics described above are illustrated in Figure 14(b) which shows the outlines of the root and tip cross-sections as viewed looking down the stacking (x-coordinate) axis.

The walls of the airfoil were idealized to be of constant thickness (approximately 0.08 in.) and comprised of 8 plies with a symmetric layup pattern of $[0/\pm 45/90]_{s}$. The composite material system for this TFRS airfoil involved 0.01 in. thick unidirectional plies composed of 0.008 in. diameter W-1.5%ThO_2 fibers in a Fe-25%Cr-4%Al-1%Y matrix such that the fiber volume

fraction was nominally 0.50. Reference properties (at room temperature) for this fiber/matrix system are summarized in Table 1. Properties for the interphase were taken to be a simple average of the fiber and matrix properties. The various material parameters required for the nonlinear TVP material relationships were evaluated, where possible, from the limited data base available on this composite material system; otherwise, the parameters were assigned arbitrary values.

4.3 Nonlinear COBSTRAN Analyses

4.3.1 Simulated Fabrication Process

The first analysis of the TFRS composite turbine blade airfoil using nonlinear COBSTRAN was conducted to examine the significance of the residual stress state induced in the airfoil when subjected to thermal loading conditions as might be imposed during a blade fabrication process. The fabrication process simulated here for the airfoil was taken from an actual hot-pressing process used to fabricate TFRS composite test specimens. The complete loading conditions for this process involve a thermal heat-up transient, a simultaneous constant-temperature/ constant-pressure transient, and a thermal cool-down transient. The analysis of the airfoil was conducted for

Table 1 - Constituent Material Properties (at Room Temperature) for TFRS Composite HPT Blade Analysis

PROPERTY	UNITS	FIBER ($WThO_2$)	MATRIX (FeCrAlY)
T_M	^oF	6164**	2690
ρ	lbf/in^3	0.697**	0.260
E_{11}	10^6 psi	52.1	30.2
E_{22}	10^6 psi	52.1*	30.2*
ν_{12}		0.29**	0.30
ν_{23}		0.29*	0.30*
α_{11}	10^{-6} in/in/^oF	2.44**	5.28
α_{22}	10^{-6} in/in/^oF	2.44*	5.28*
S_{11T}	ksi	410	127
S_{22T}	ksi	410*	127*
S_{12}	ksi	246*	76*

* assumed value

** value from handbook for pure tungsten

the thermal cool-down transient only since the initiation of cooling was judged to be a reasonable point in the fabrication process to assume the onset of composite behavior for the plies and the laminate.

In the fabrication thermal cooling process, temperature is decreased from 2000^{o}F to room temperature (70^{o}F) over a 16-hour period. For the analysis the thermal cool-down transient was approximated as seen in Figure 15 using 10 load/time increments. The temperature was assumed to be uniformly distributed over the airfoil (inner and outer surfaces) such that every ply at every node experienced the same thermal load.

The boundary conditions for the analysis were defined so as to minimize constraint. Each node at the root cross-section (see Figure 14) of the airfoil was restrained against translation in the x-direction. In addition, the node at the root trailing edge was restrained against translation in the y- and z-direction (completely pinned).

The analysis of the thermal cool-down transient was conducted on a CRAY 1S computer system and required approximately 12 minutes of CPU time. A tolerance of 5% was prescribed for the equilibrium-solution convergence criterion for each load/time increment. Convergence was achieved in two iterations for each load/time increment

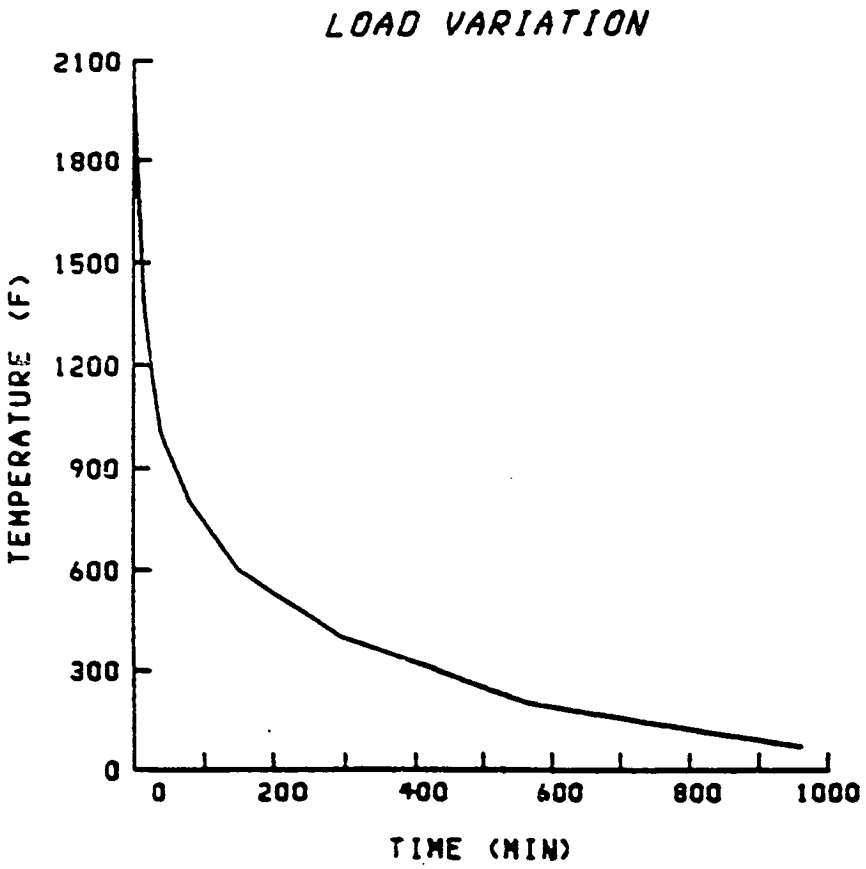

Figure 15 - Thermal Cool-down Transient for Fabrication Process

with a maximum error of -3.6% occurring for the first increment and a minimum error of 0.1% occurring for the tenth increment.

Results from the analysis of the simulated fabrication process indicated a uniform (for all practical purposes) state of ply residual stress throughout the airfoil, as might have been expected due to the uniform quasi-isotropic ply configuration and uniform temperature distribution. Overall, the values for ply longitudinal normal stress ($\sigma_{\ell 11}$) varied from approximately -10.5 ksi to -12.5 ksi, with the majority of values falling in the range -11.5 $\pm$ 0.3 ksi. The values for transverse normal stress ($\sigma_{\ell 22}$) were similar in range and magnitude to the values for $\sigma_{\ell 11}$ but opposite in sense (i.e. tensile rather than compressive). Results also indicated small shear stresses ($\sigma_{\ell 12}$) ranging in value from approximately 0.0 to $\pm$1.0 ksi with no regular pattern of distribution. The small shear stresses and the variations in normal stresses were attributed to a combination of cumulative numerical error and small-scale bending/torsion in the airfoil due to the asymmetric airfoil geometry and the imposed boundary conditions. To illustrate the types of local information provided by nonlinear COBSTRAN pertaining to the change in state of a ply and its constituents, results of the analysis are presented below

for the outermost 0^{o} ply (ply no. 1) at the root trailing edge node (node no. 1) of the discretized airfoil model (see Figure 14).

One of the characteristics which makes this particular fiber/matrix system attractive as a first-generation TFRS composite turbine blade material is the excellent chemical compatibility between the $WThO_2$ fibers and the FeCrAlY matrix. This characteristic is illustrated in Figure 16 which shows the negligible amount of fiber degradation that occurred in the ply during the cooling portion of the fabrication process. At the end of the thermal cool-down transient, the results of the analysis indicated approximately 0.1% of the fiber cross-sectional area had been degraded.

One indication of the state of a ply and its constituents is given in terms of stress fields. The build-up of longitudinal normal residual stress (σ_{l11}) in the ply during the fabrication cooling process is shown in Figure 17 together with the corresponding distribution of longitudinal normal residual microstresses in the constituents. Despite the relatively small magnitude of ply residual stress, the magnitudes of microstresses in the constituents are significantly higher due to the difference in thermal expansion coefficients between the constituents. The tensile nature of the matrix microstress and compressive nature of the fiber

NODE NO. 1
PLY NO. 1

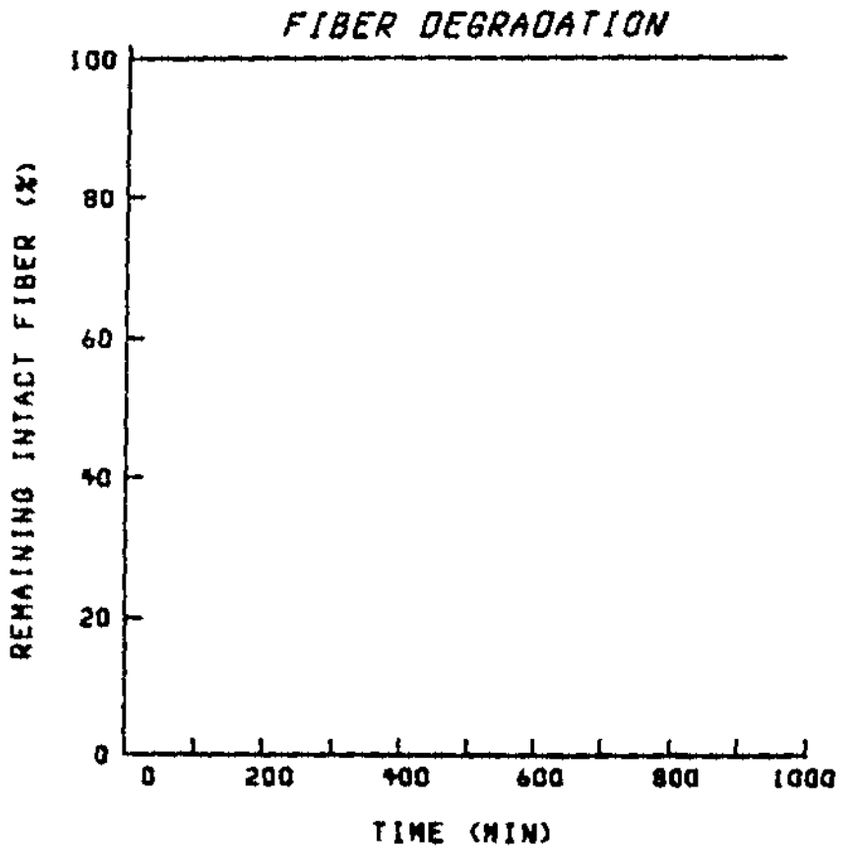

Figure 16 - Fiber Degradation for Fabrication Process (Node 1/Ply 1)

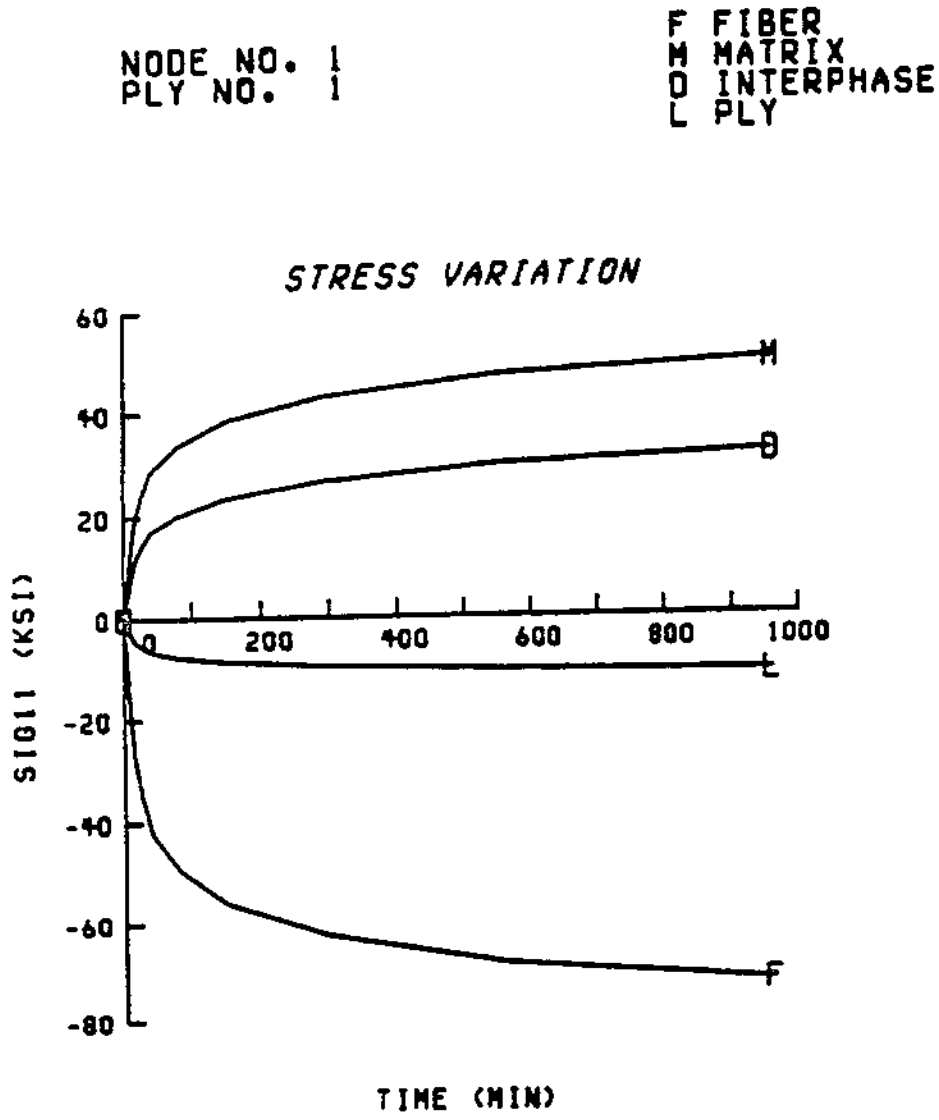

Figure 17 - Build-up of Longitudinal Normal Residual Stress (σ_{11}) for Fabrication Process (Node 1/Ply 1)

microstress results from the fact that the matrix has the larger coefficient of thermal expansion. Similar results are shown in Figure 18 indicating the build-up of transverse normal residual stress (σ_{22}) in the ply and the resulting distribution of residual microstresses in the constituents. The results in Figure 18 illustrate one of the physical complexities associated with this problem, as discussed earlier, regarding the nonuniformity of constituent transverse microstresses through-the-thickness of the ply. Note the variation of microstress for the matrix and interphase for the different regions or zones. Again, despite the relatively small ply residual stress magnitude, the magnitudes of the constituent microstresses are significantly higher because of the difference in thermal expansion coefficients between the constituents.

Another indication of the change in state of the ply and its constituents, in terms of material properties, is illustrated in Figure 19 which shows the variation of longitudinal normal modulus (E_{11}) during the fabrication cooling process. To explain the results shown in Figure 19 for the constituents, it is necessary to recall the form of the nonlinear TVP material relationships discussed in Chapter 2 (see Figure 4). In the case of the matrix, the modulus increased with the initiation of the cooling process, as might have been expected. This reflects a

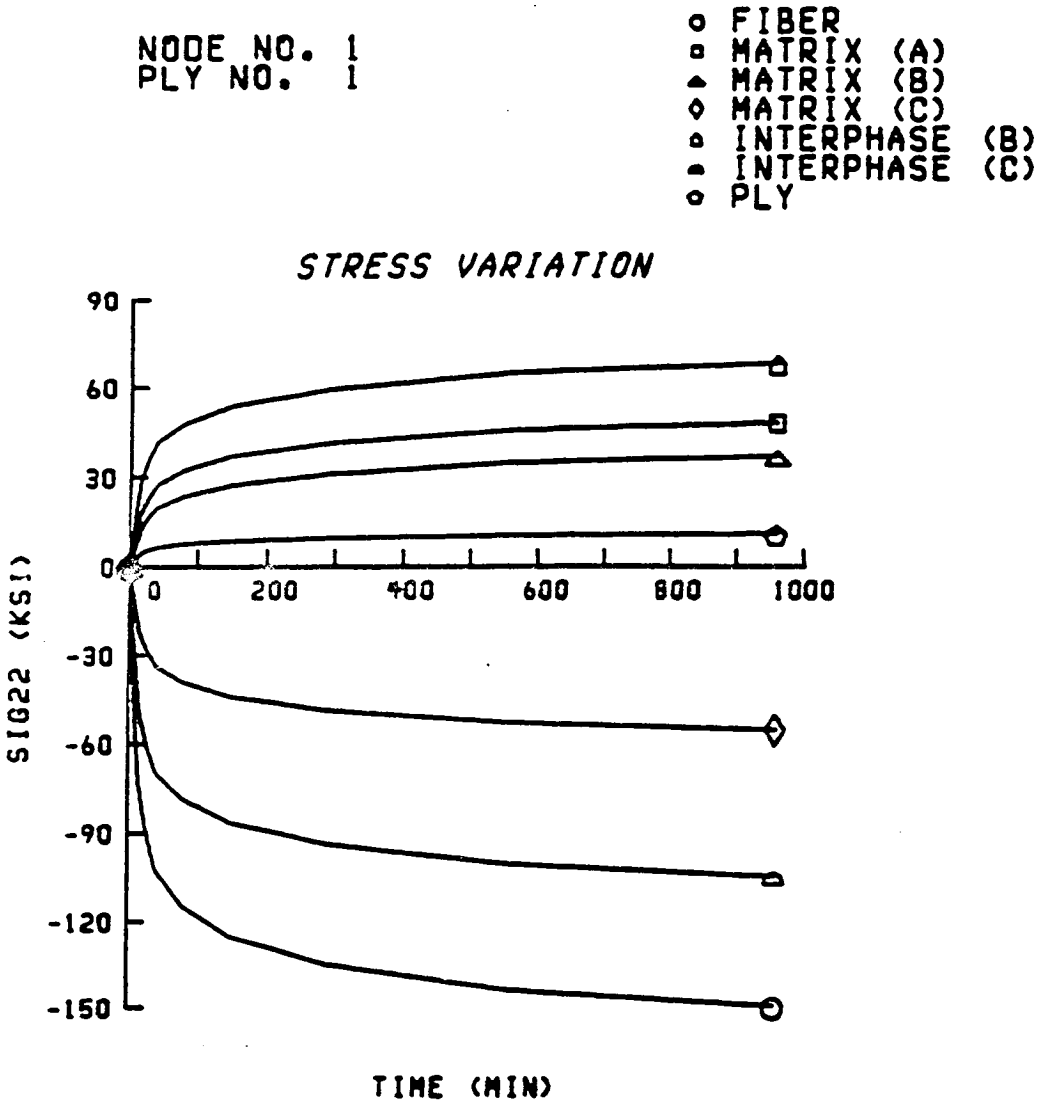

Figure 18 - Build-up of Transverse Normal Residual Stress (σ_{22}) for Fabrication Process (Node 1/Ply 1)

NODE NO. 1
PLY NO. 1

F FIBER
M MATRIX
D INTERPHASE
L PLY

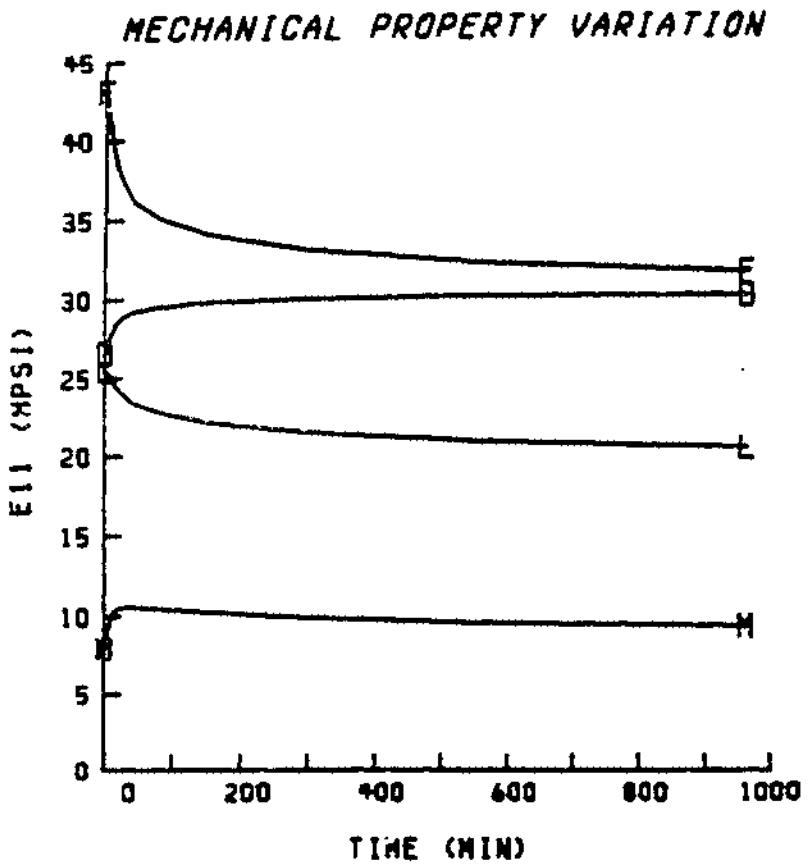

Figure 19 - Variation of Longitudinal Normal Modulus (E_{11}) for Fabrication Process (Node 1/Ply 1)

dominance of the material property temperature-dependency, as expressed in the first term of the nonlinear TVP material relationship for constituent mechanical properties (first expression, Figure 4). However, with the build-up of longitudinal normal residual microstress in the matrix, the material property stress-dependency became increasingly more significant until its effect virtually balanced the temperature-dependency, resulting in the abrupt leveling-off of the matrix modulus as seen in Figure 19. The same rationale holds for the behavior of the interphase modulus, whereas the behavior of the fiber modulus was dominated by the material property stress-dependency from the outset. The value for ply modulus is based on the composite micromechanics equation. It should be remembered that the predicted constituent material property behavior is highly sensitive to the various material parameters in the nonlinear TVP relationships. As such, and in view of the fact that insufficient data was available to evaluate all the material parameters for this analysis (most were estimated), the trends of material property behavior indicated here are probably not realistic. Nevertheless, the results demonstrate the capability of nonlinear COBSTRAN to trace the nonlinearity in the integrated sense, from the microscopic level to the global level and

back, and capture the trends of nonlinear material behavior at the constituent level. Results similar to those just presented for E_{11} are shown in Figure 20 for transverse normal modulus (E_{22}). The fiber and interphase moduli are affected more significantly by the material property stress-dependency, which follows from the transverse normal microstress state shown earlier (Figure 18).

An example of ply and constituent thermal property behavior is given in Figure 21 which shows the variation of longitudinal thermal expansion coefficient (α_{11}) during the fabrication cool-down transient. Thermal properties were initially assumed to be primarily temperature dependent inasmuch as the limited database available for this composite material system contained only temperature-dependency information for the constituent thermal properties. As such, the exponents for the stress- and rate-dependency terms (the second and third terms) of the nonlinear TVP material relationship for constituent thermal properties (second expression, Figure 4) were intentionally assigned small values to cause the relative effects of these two terms to be insignificant. This assumption is reflected in the results shown in Figure 21. Again, the thermal expansion coefficient for the ply is based on the composite micromechanics equation.

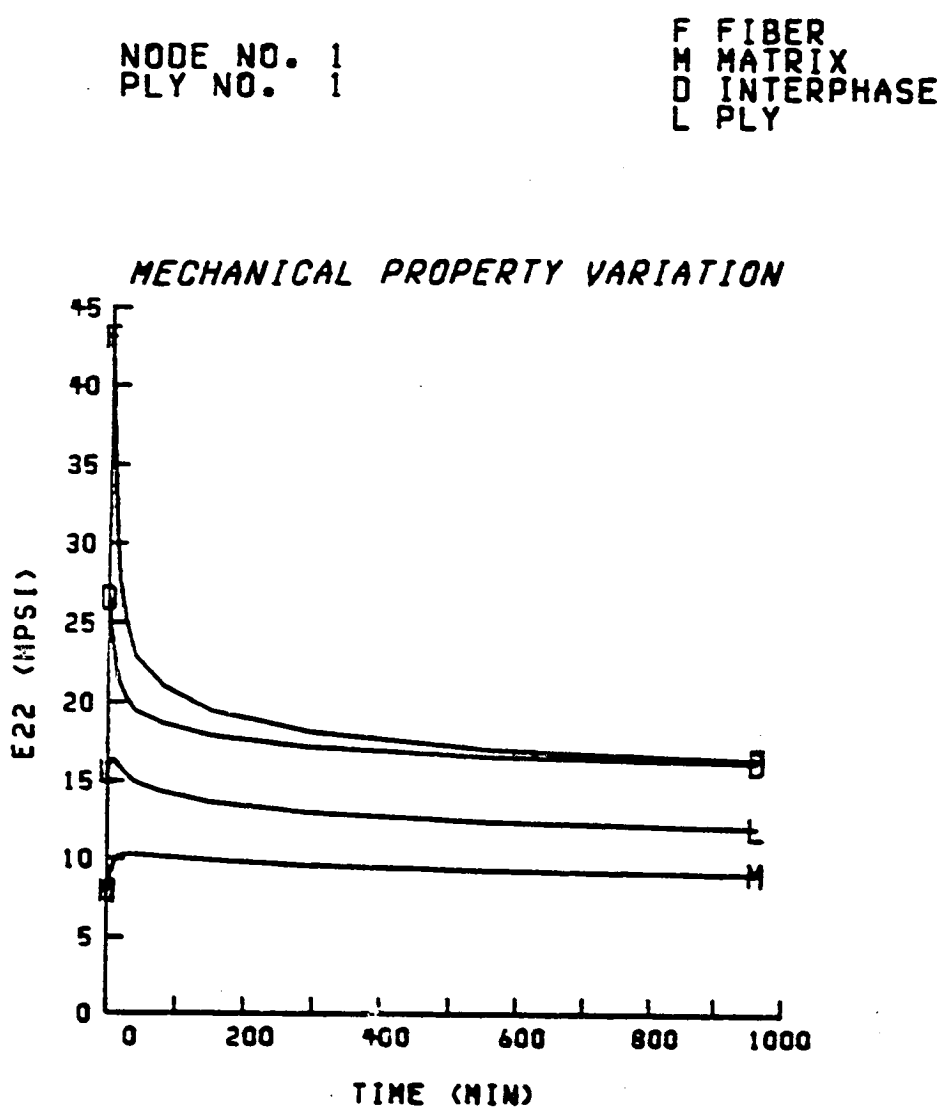

Figure 20 - Variation of Transverse Normal Modulus (E_{22}) for Fabrication Process (Node 1/Ply 1)

NODE NO. 1
PLY NO. 1

F FIBER
M MATRIX
O INTERPHASE
L PLY

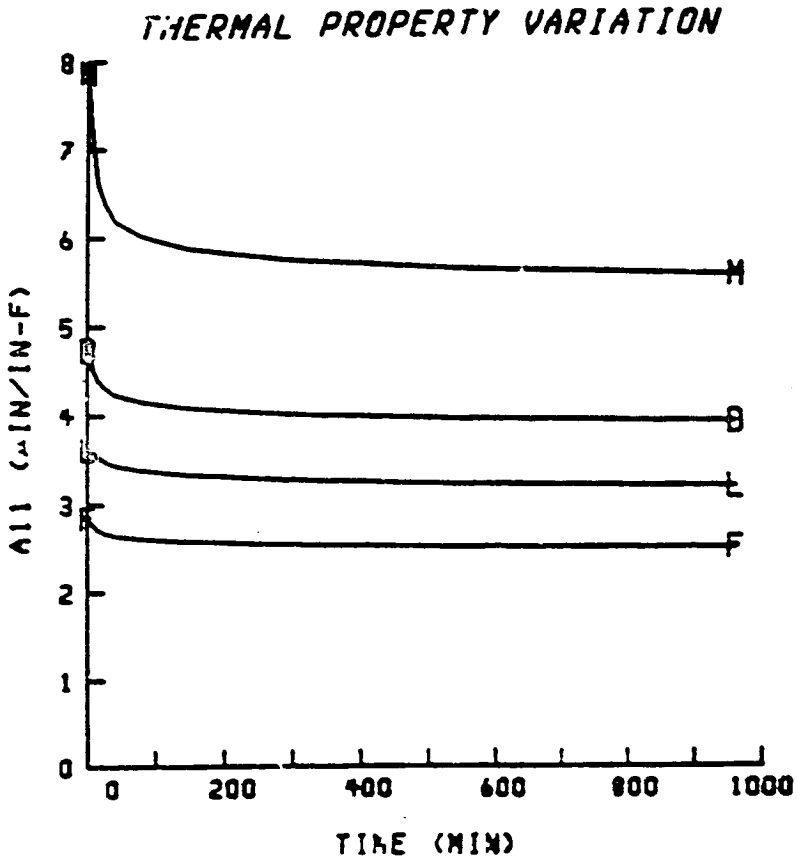

Figure 21 - Variation of Longitudinal Thermal Expansion Coefficient (α_{11}) for Fabrication Process (Node 1/Ply 1)

Finally, an example of ply and constituent uniaxial strength behavior is given in Figure 22 which shows the variation of longitudinal tensile strength during the fabrication cooling process. The results shown in Figure 22 reflect primarily a temperature-dependency of constituent strengths. Again, because of the inadequate database available for this material system, the coefficients for the fatigue-like and creep-like terms (logarithmic terms) in the nonlinear TVP relationship for constituent residual strengths (third expression, Figure 4) were intentionally assigned small values to cause the relative effects of these terms to be less significant. The predicted ply strength in Figure 22 is based on the corresponding composite micromechanics equation.

4.3.2 Simulated Engine Mission

The second analysis of the TFRS composite turbine blade airfoil using nonlinear CORSTRAN was conducted to investigate the response of the airfoil to a simulated engine mission. The residual stress state and material state of the airfoil resulting from the analysis of the simulated fabrication process were taken as initial conditions for the engine mission analysis.

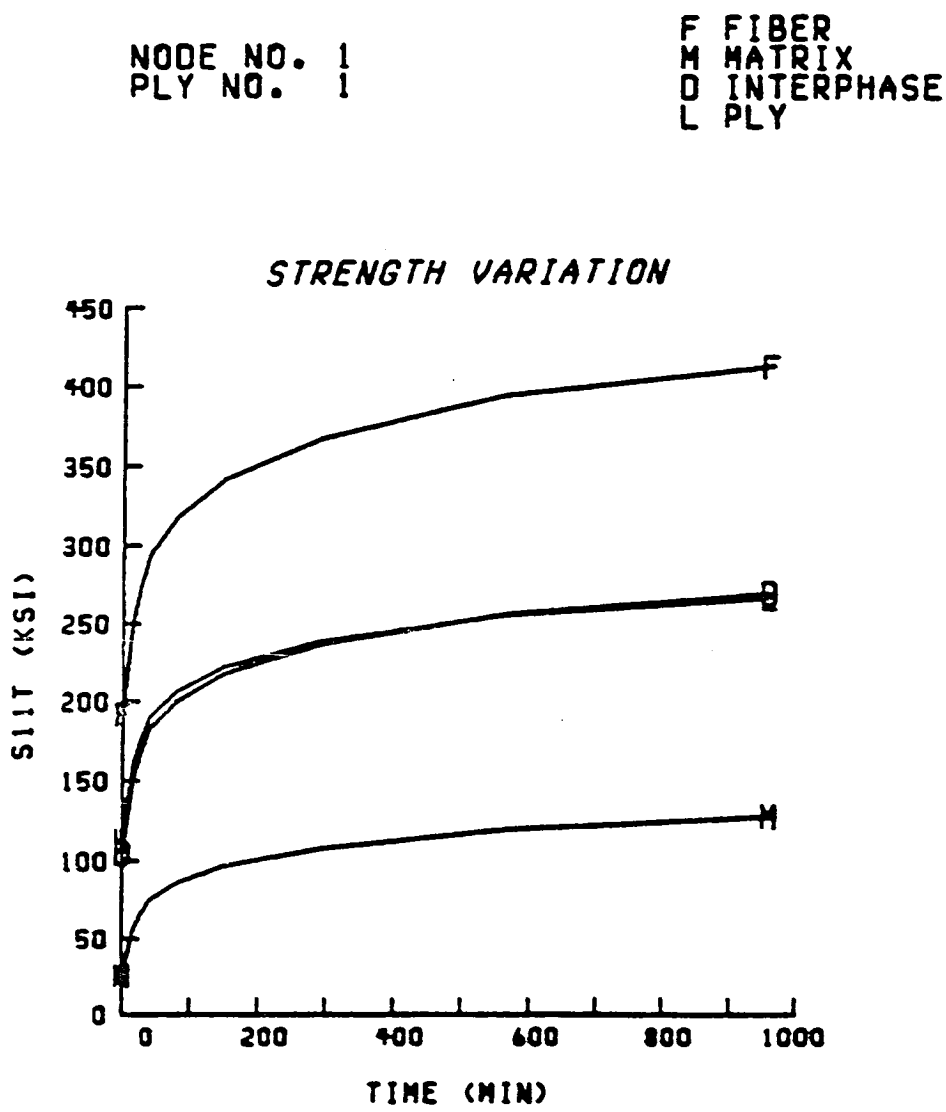

Figure 22 - Variation of Longitudinal Tensile Strength (S_{11T}) for Fabrication Process (Node 1/Ply 1)

The complete simulated engine mission was comprised of; a 20-second take-off transient, a 2-minute climb transient, a 40-minute cruise transient, a 5-minute descent transient, a 20-second landing transient, and a 20-minute cool-down transient. The loading conditions for the mission consist of time-varying temperature, pressure, and centrifugal force fields. The temperature and pressure fields were assumed to have a bicubic distribution (cubic spanwise and chordwise) over the exterior surfaces (pressure and suction sides) of the airfoil. Furthermore, the airfoil was assumed to be uncooled such that there was no thermal gradient through-the-thickness of the airfoil walls and no interior airfoil pressure. The maximum loading condition for the engine mission was assumed to result from the simultaneous occurrence of the maximum of each individual load (temperature, pressure and centrifugal force) and occur at the end of the take-off transient. The airfoil exterior surface temperature/pressure distributions for the maximum loading condition is summarized in Table 2.

The boundary conditions imposed on the airfoil for the analysis most closely represented the airfoil as a cantilevered structure. The nodes at the root cross-section of the airfoil were restrained against x-translation and x- and y-rotation. The node at the

Table 2 - HPT Blade Maximum Airfoil Temperature/Pressure Distributions for Simulated Engine Mission

SPAN LOCATION	SURFACE	CHORD LOCATION		
		LEADING EDGE	MID-CHORD	TRAILING EDGE
ROOT	SUCTION	1550/103	1520/70	1540/42
	PRESSURE	1550/147	1520/100	1540/60
MID-SPAN	SUCTION	1950/131	1880/70	1920/61
	PRESSURE	1950/187	1880/100	1920/87
TIP	SUCTION	1430/140	1390/79	1410/112
	PRESSURE	1430/200	1390/113	1410/160

trailing edge of the root cross-section was also restrained against y- and z-translation.

For the analysis, the engine mission was approximated by 26 load/time increments. A tolerance of 10% was prescribed for the equilibrium-solution convergence criterion for the load/time increments. The analysis was conducted on a CRAY 1S computer system and required approximately 40 minutes of CPU time. An equilibrium solution was achieved for all load/time increments except the 24^{th} which, after a prescribed maximum of 10 iterations, converged to an error of 12%. In view of the fact that this analysis was conducted for demonstration purposes only, no actions were taken to reduce this error to within the tolerance limit. Normally, the load/time increment would be subdivided to reduce the error and achieve a better solution.

Results from the analysis indicated a residual stress state in the plies at the end of the mission which was significantly different from the initial ply residual stress state. Generally, the difference varied depending on the component of ply stress and the location on the airfoil. For example, the difference was least significant at the tip of the airfoil as might be expected since the effects of centrifugal force loading and global bending due to pressure loading vanish at the tip.

The longitudinal normal ply residual stresses ($\sigma_{\ell 11}$) at the tip of the airfoil changed only slightly in magnitude from before the engine mission to after the engine mission and remained relatively uniform through-the-thickness of the airfoil walls. Moreover, the magnitude of $\sigma_{\ell 11}$ for the two center plies (90^{o}) showed only slight variation with position (spanwise and chordwise) on the airfoil. However, the through-the-thickness variation of $\sigma_{\ell 11}$ was increasingly nonuniform (but relatively symmetric) in moving from tip to root with the nonuniformity being most pronounced near mid-chord rather than at the leading or trailing edge. The magnitude of $\sigma_{\ell 11}$ was maximum for the center plies of the airfoil walls and decreased symmetrically from the center plies to the surface plies. In the area of the airfoil near the root and near the mid-chord, $\sigma_{\ell 11}$ for the inner and outer surface plies of the airfoil walls changed from compressive to tensile. The chordwise sensitivity of the through-the-thickness variation of $\sigma_{\ell 11}$ is attributed to the effects of local bending of the airfoil walls due to pressure loading.

As was the case with $\sigma_{\ell 11}$, the transverse normal ply residual stresses ($\sigma_{\ell 22}$) at the tip of the airfoil changed only slightly from before the engine mission to after the engine mission and remained relatively uniform through-the-thickness of the airfoil walls. Different

from $\sigma_{\ell 11}$, however, the magnitudes of $\sigma_{\ell 22}$ for the center plies (90°) of the airfoil walls showed the greatest variation in moving from tip to root while the surface plies (0°) showed only slight variation. Again, as with $\sigma_{\ell 11}$, the through-the-thickness variation of $\sigma_{\ell 22}$ was increasingly nonuniform (but relatively symmetric) in moving from tip to root with the nonuniformity being most pronounced near mid-chord. Moreover, the magnitude of $\sigma_{\ell 22}$ was maximum for the cent plies and decreased symmetrically from the center plies to the surface plies.

Ge. ally, the in-plane shear ply residual stress ($\sigma_{\ell 12}$) behaved in a manner similar to the transverse normal stress. The magnitude of $\sigma_{\ell 12}$ was maximum, however, for the $\pm 45^{\circ}$ plies.

Overall, the maximum value of $\sigma_{\ell 11}$ was -13.3 ksi and occurred in one of the center plies (90°) at the root trailing edge (node 1, see Figure 14) of the airfoil. The maximum values of $\sigma_{\ell 22}$ and $\sigma_{\ell 12}$ were 26.6 ksi and 7.1 ksi, respectively and occurred at the same location mid-chord on the suction side of the airfoil (node 15, see Figure 14). The maximum value of $\sigma_{\ell 22}$ occurred in one of the center (90°) plies and the maximum value of $\sigma_{\ell 12}$ occurred in the outermost $+45^{\circ}$ ply.

Results from the analysis of the simulated engine mission also indicated a permanent set of the airfoil as given by the cumulative nodal displacements at the end of the mission. This permanent set resulted in a very slight tilting (approximately 0.04^{o}), untwisting (approximately 0.05^{o}) and axial growth (approximately 0.01 in. at the tip) of the airfoil.

Similar to the examples shown previously for the analysis of the simulated fabrication process, examples of results for the analysis of the simulated engine mission are given below to illustrate the local information provided by nonlinear COBSTRAN pertaining to the change in state of a ply and its constituents. Again, the results are for the outermost ply (ply no. 1) at the root trailing edge point (node no. 1) of the airfoil (see Figure 14).

The loads experienced at this particular node/ply location on the airfoil are illustrated in Figures 23-25 which show the variation of temperature, pressure and engine speed during the simulated engine mission. Note that the temperature load exists throughout the entire mission while the pressure and centrifugal force (due to engine speed) loads exist only to the end of the landing transient.

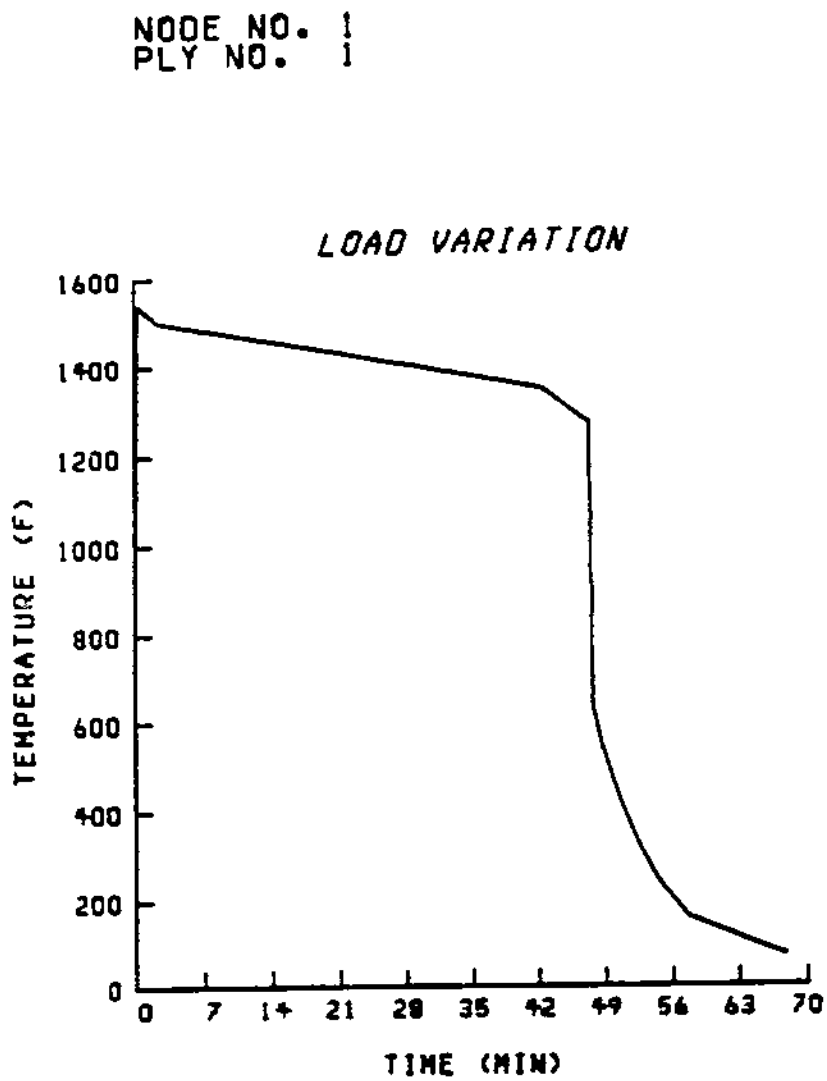

Figure 23 - Variation of Temperature Load for Engine Mission (Node 1/Ply 1)

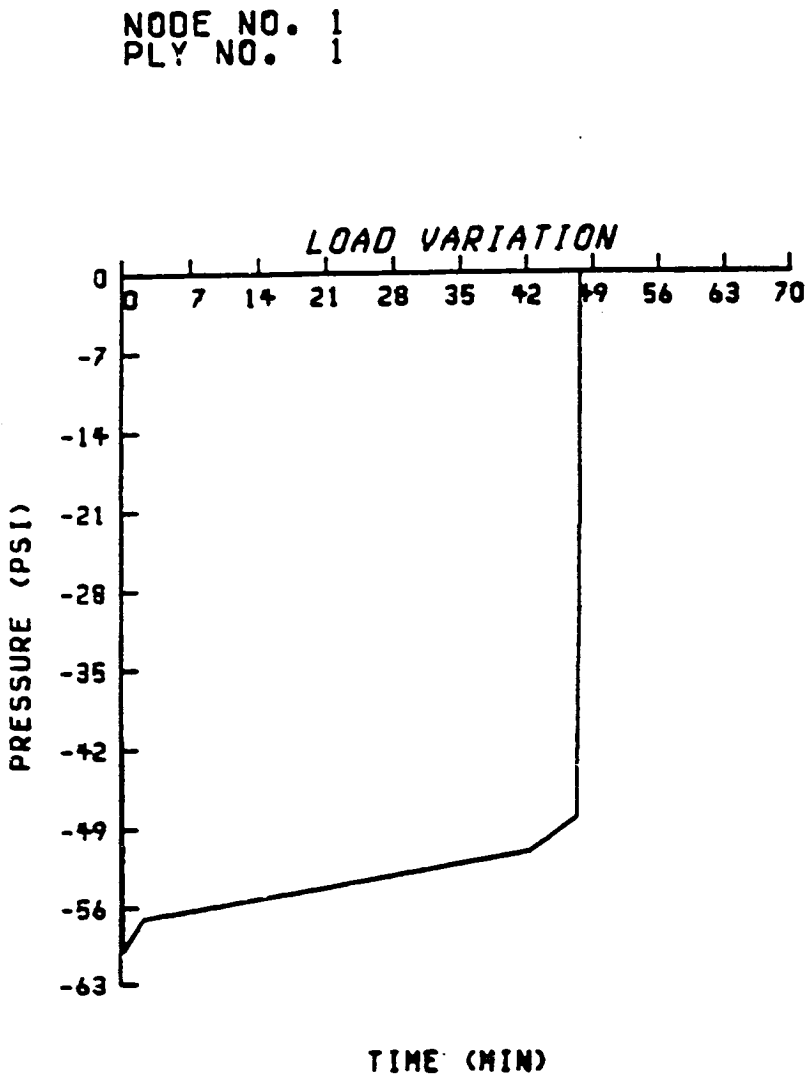

Figure 24 - Variation of Pressure Load for Engine Mission (Node 1/Ply 1)

NODE NO. 1
PLY NO. 1

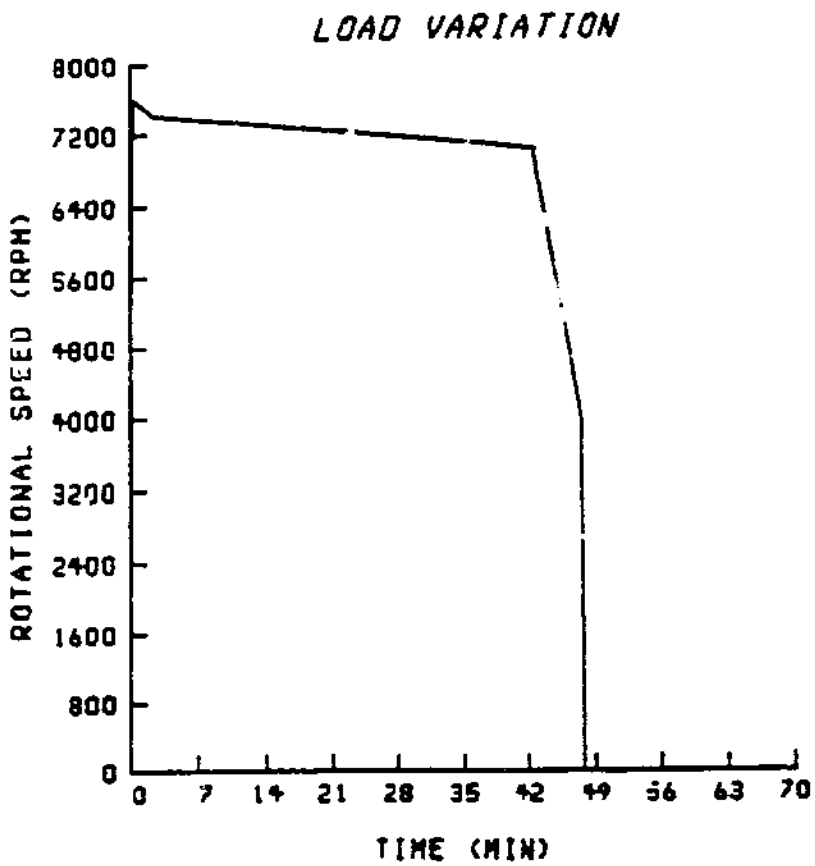

Figure 25 - Variation of Engine Speed for Engine Mission

The variation of longitudinal normal stress (σ_{11}) in the ply and the corresponding distribution of longitudinal normal microstresses in the constituents are shown in Figure 26. The magnitude of residual stress in the ply at the end of the mission is slightly less than the initial value. The magnitude of residual microstress in the fiber is somewhat lower than the initial value whereas that of the matrix is slightly higher. Similar results are shown in Figure 27 for the variation of transverse normal stress (σ_{22}) in the ply and the corresponding distribution of transverse normal microstresses in the constituents. The most significant differences from initial to final values of microstress occur in the fiber and in the matrix and interphase in the C-region. These particular microstresses also show the most significant fluctuation throughout the mission. Note that during this mission, the matrix and interphase microstress components in the C-region change from compressive to tensile and back to compressive. Finally, similar results are shown in Figure 28 for the variation of in-plane shear stress (σ_{12}) for the ply and the corresponding distribution of in-plane shear microstresses in the constituents. Again, there is a distinct difference in values from initial to final state, most noticeably for the fiber.

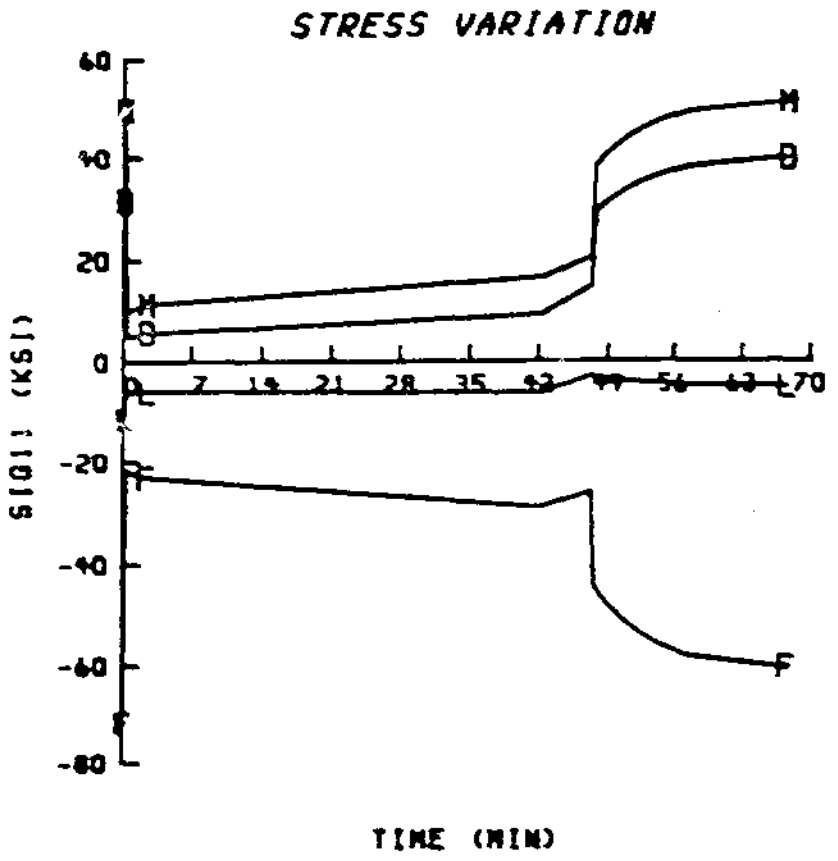

Figure 26 - Variation of Longitudinal Normal Stress (σ_{11}) for Engine Mission (Node 1/Ply 1)

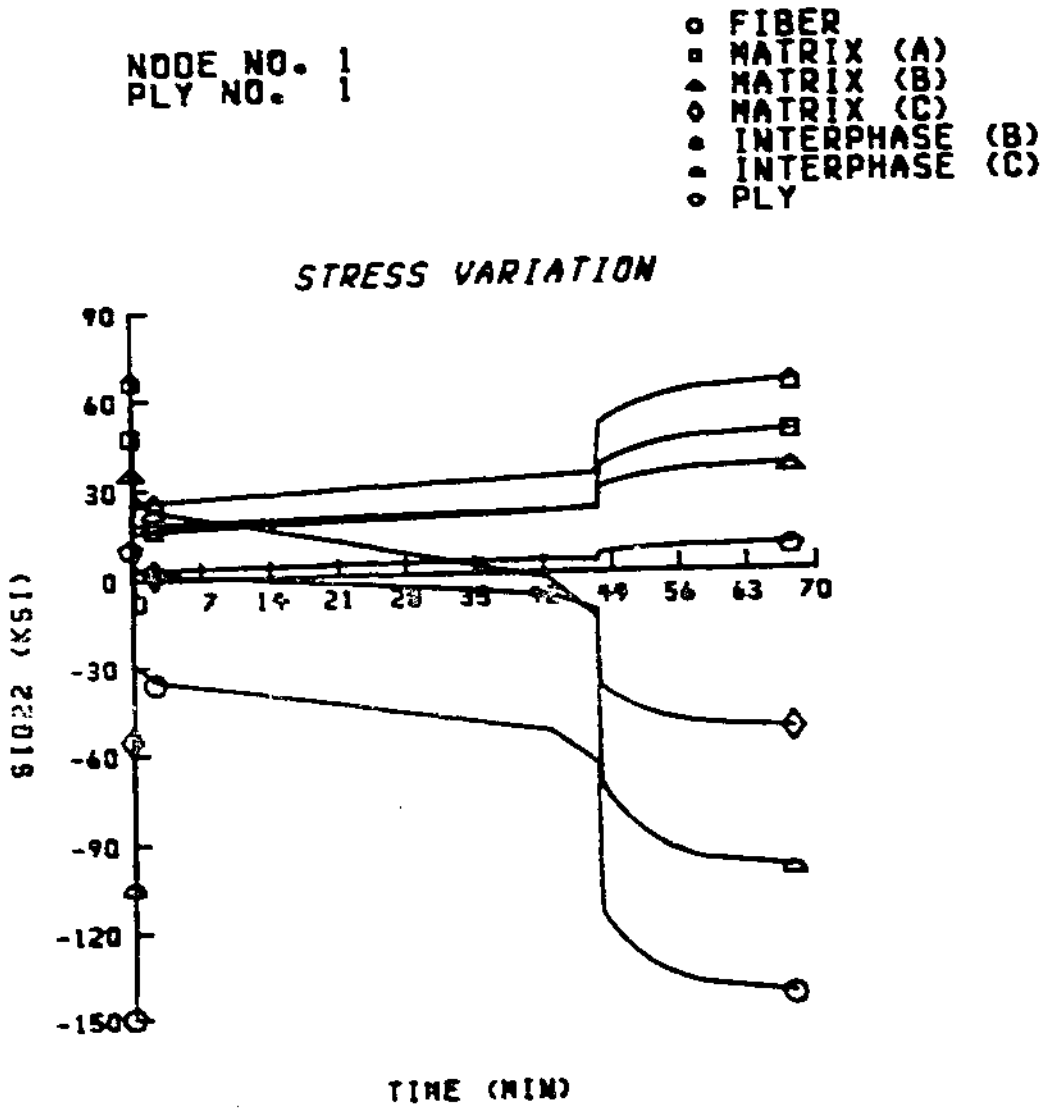

Figure 27 - Variation of Transverse Normal Stress (σ_{22}) for Engine Mission (Node 1/Ply 1)

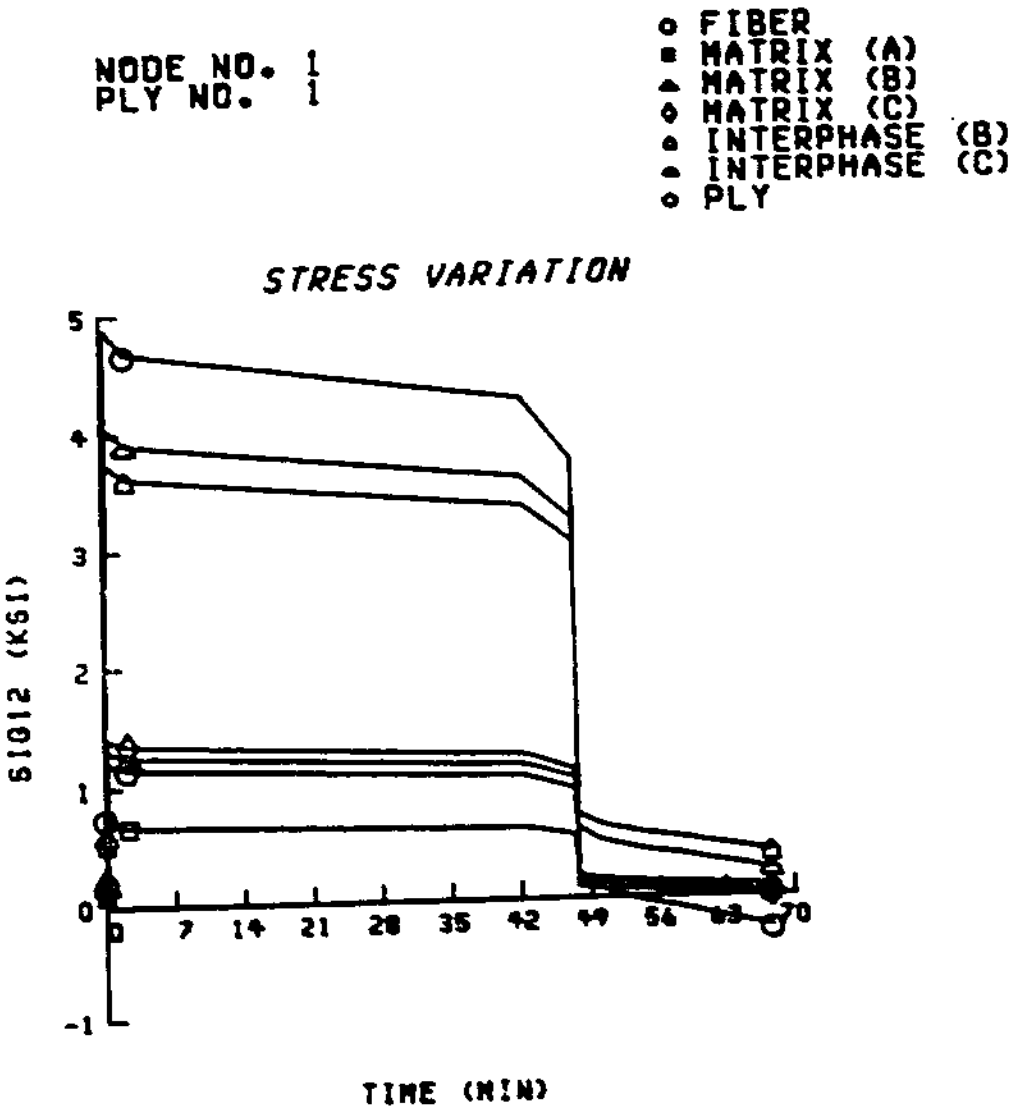

Figure 28 - Variation of In-plane Shear Stress (σ_{12}) for Engine Mission (Node 1/Ply 1)

The change in state of the ply and its constituents, in terms of a change in material properties, is illustrated in Figure 29 which shows the variation of longitudinal normal modulus (E_{11}) during the simulated engine mission. Note the behavior of the fiber modulus during the take-off transient portion of the mission. Despite a sharp increase in temperature (see Figure 23) during the take-off transient, the fiber modulus displays an increase in magnitude, contrary to what might be expected. This response is attributed to the fact that, during the take-off transient, the magnitude of the longitudinal normal component of microstress in the fiber (see Figure 26) decreased substantially. This behavior reflects a dominance of the material property stress-dependency as expressed in the first term of the nonlinear TVP material relationship for mechanical properties (see Figure 4). The behavior of the fiber modulus throughout the remainder of the mission follows the same pattern. Similarly, the same reasoning holds for the behavior of the matrix modulus, however, the relative effects of the temperature-dependency and stress-dependency on the behavior were more balanced. The behavior of the interphase modulus, on the other hand, was dominated by the temperature-dependency, but again, the relative effects of temperature- and stress-dependency

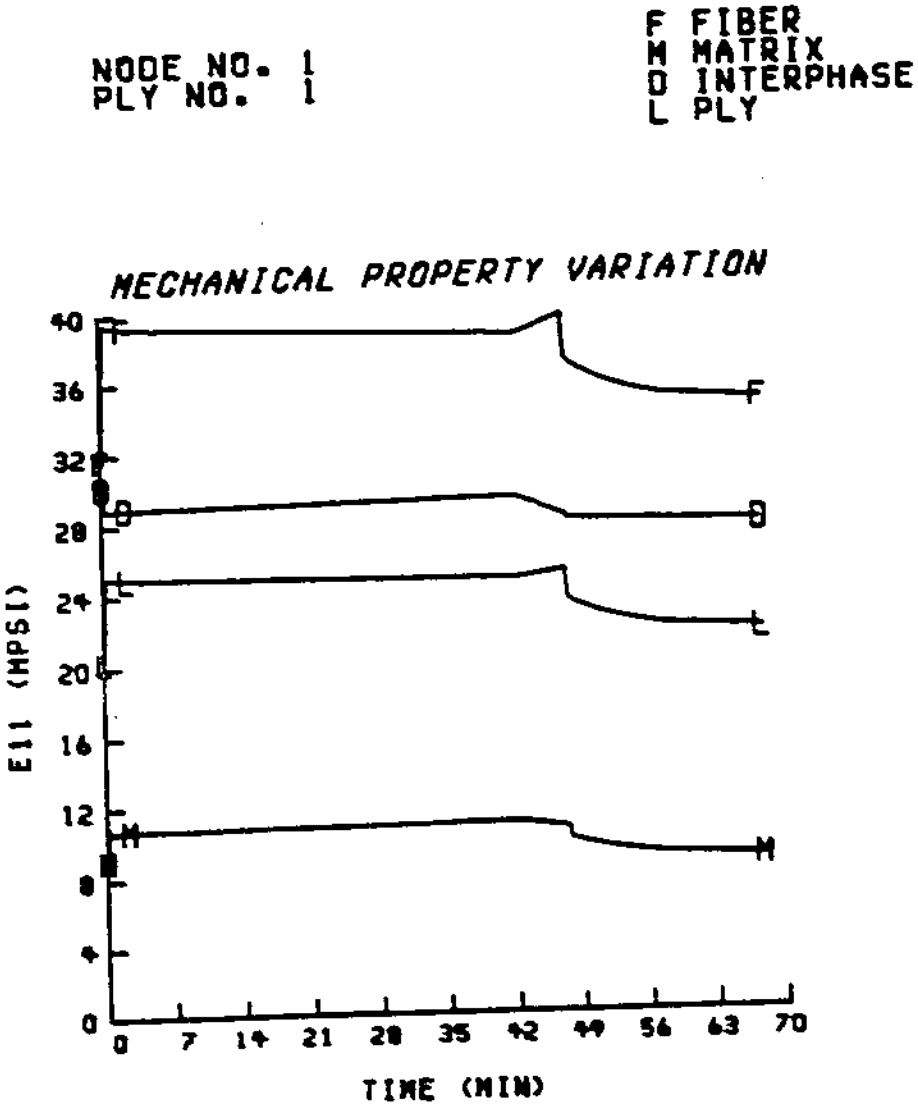

Figure 29 - Variation of Longitudinal Normal Modulus (E_{11}) for Engine Mission (Node 1/Ply 1)

were more balanced. Overall, the modulus of the ply, as predicted by the corresponding composite micromechanics equation, shows an improvement from the beginning to the end of the engine mission.

Results similar to those just presented for E_{11} are given in Figures 30-32 for transverse normal modulus (E_{22}), longitudinal thermal expansion coefficient (α_{11}), and longitudinal ultimate tensile strength (S_{11T}). The behavior of E_{22} is analogous to the behavior of E_{11}. As mentioned in the discussion of results from the analysis of the simulated fabrication process, α_{11} and S_{11T} were taken to be primarily temperature-dependent because of the insufficient database available for this material system to evaluate the stress- or rate-dependency. The behavior of α_{11} and S_{11T}, as modelled by the nonlinear TVP material relationships, reflects this assumption as illustrated in Figures 31 and 32.

NODE NO. 1
PLY NO. 1

F FIBER
M MATRIX
D INTERPHASE
L PLY

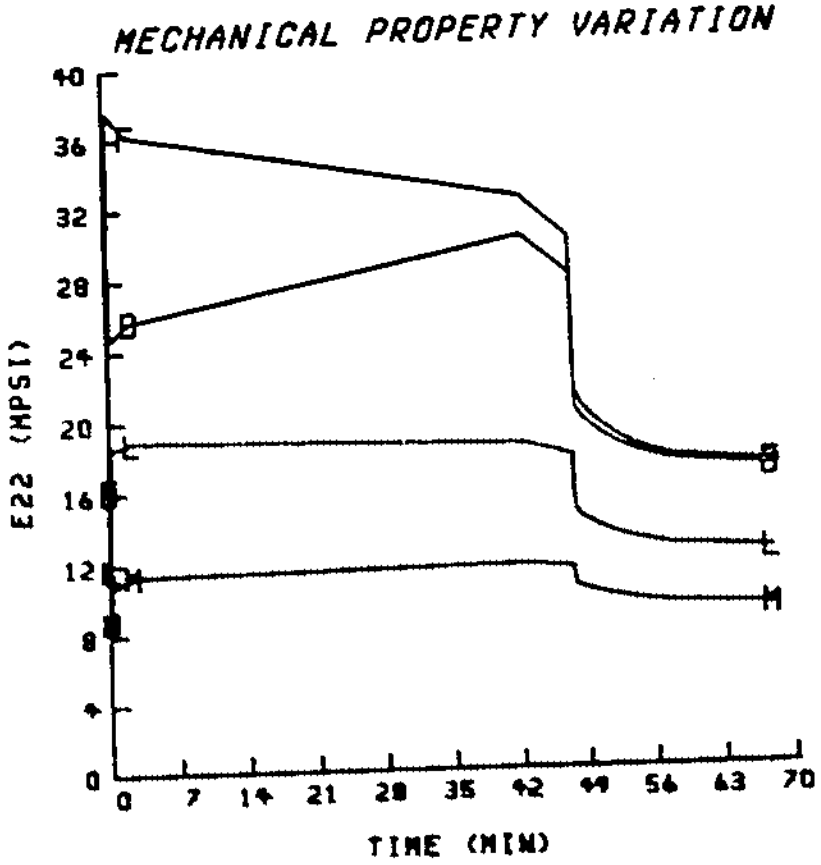

Figure 30 - Variation of Transverse Normal Modulus (E_{22}) for Engine Mission (Node 1/Ply 1)

NODE NO. 1
PLY NO. 1

F FIBER
M MATRIX
D INTERPHASE
L PLY

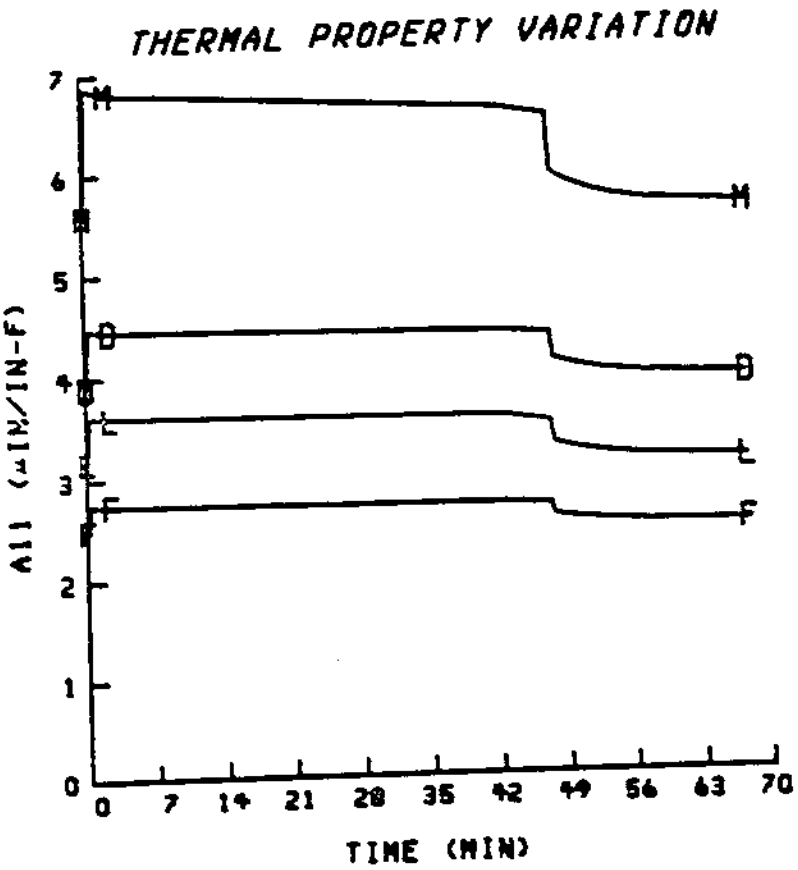

Figure 31 - Variation of Longitudinal Thermal Expansion Coefficient (α_{11}) for Engine Mission (Node 1/ Ply 1)

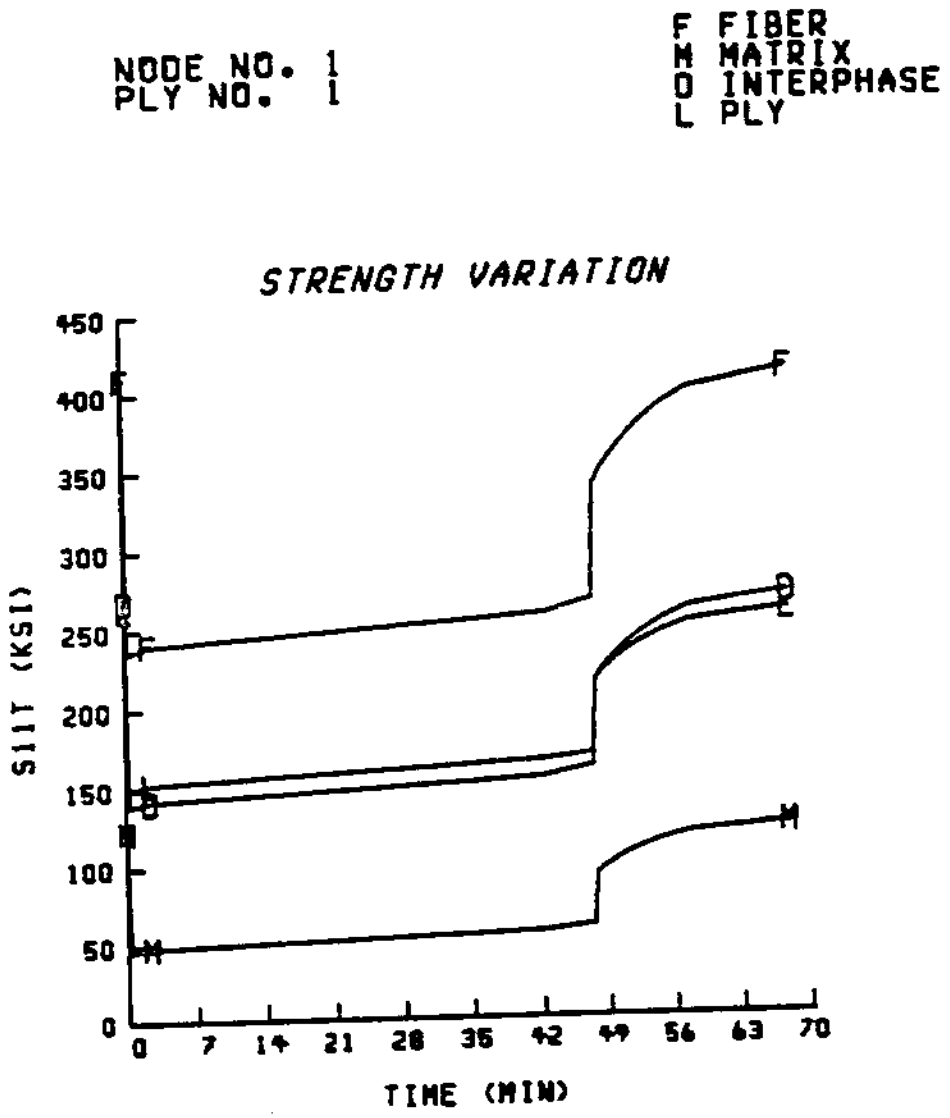

Figure 32 - Variation of Longitudinal Tensile Strength (S_{11T}) for Engine Mission (Node 1/Ply 1)

CHAPTER 5

SUMMARY

Strictly speaking, the subject of this thesis has been the research conducted, to date, toward the development of a specialized structural/stress analysis capability specifically tailored for the nonlinear analysis of tungsten-fiber-reinforced superalloy (TFRS) composite high-pressure turbine (HPT) blade/vane components. This effort was necessitated by a general unavailability of appropriate and adequate methods with which to make a quantitative assessment of the mechanical performance and structural integrity of this (or any) advanced high-temperature composite for this (or any) aircraft gas turbine engine application.

The emphasis in developing a specialized analytical capability for TFRS composite turbine blade/vane components has been to account for the complex physics associated with this application, including; nonlinear and anisotropic material behavior, micro- and macro-inhomogeneity, and fiber degradation. This effort resulted in the development of a special purpose

computerized structural analysis package (nonlinear COBSTRAN) which incorporates the required fiber degradation model, nonlinear thermoviscoplastic (TVP) material relationships, composite micromechanics theory, laminate theory, and global structural analysis to relate the local nonlinear behavior of the TFRS constituent materials to the global response of a turbine blade/vane component. The solution strategy of nonlinear COBSTRAN is based on an approach (upward-integrated top-down-structured analysis) which, in itself, is completely general and provides the conceptual framework whereby specialized analytical tools can be developed for virtually any composite structural application.

The key theoretical aspects and major computer programming efforts involved in the development of nonlinear COBSTRAN were discussed. A demonstration problem was provided to manifest the utility of the general approach and to illustrate the current capabilities of nonlinear COBSTRAN. The demonstration problem involved analyses of a hypothetical TFRS composite HPT turbine airfoil for a simulated fabrication process and a simulated engine mission. Based on the preliminary results of the demonstration problem, it is concluded that;

1. The upward-integrated top-down-structured strategy is a viable and feasible approach for composite structural analysis, in general.

2. As implemented in nonlinear COBSTRAN, this approach provides the capability to trace material history in a structure from fabrication through successive missions.

3. The capabilities of nonlinear COBSTRAN succeed in capturing trends of local nonlinear (stress-temperature-time dependent) and anisotropic material behavior. This local material behavior is related to the global response of a structure through the upward-integrated process. In turn, the global response of the structure is related back to the local material behavior through the top-down-structured process.

Development of nonlinear COBSTRAN was undertaken as an evolutionary task. At present, this special purpose analytical capability is an unproven developmental tool. To what extent nonlinear COBSTRAN succeeds in accounting for the actual physics associated with the application of TFRS composites in HPT blade/vane components remains to be investigated. As a future effort, it is intended that nonlinear COBSTRAN be "fine-tuned" through a comprehensive program of experimental testing and theoretical methodology refinement.

Based on the overall experience accrued in carrying out this research, the following recommendations are made;

1. The general upward-integrated top-down-structured approach for composite structural analysis should be implemented in a small-scale, totally self-contained research finite element code.

2. This research code should be streamlined for the incremental/iterative solution strategy imbedded in the upward-integrated top-down-structured approach.

3. The code should be highly modular and flexible to facilitate incorporation of future developments, such as; alternate material models, alternate micromechanics theories for composites other than the fiber-reinforced type, higher-order laminate theories, alternate finite element formulations, etc.

4. Preprocessing and postprocessing chores should be handled independently of the analysis.

5. The code should make use of state-of-the-art computer programming techniques and algorithms to optimize computer resource efficiency.

REFERENCES

REFERENCES

1. P. Melnyk and J. N. Fleck, "Tungsten Wire-Reinforced Superalloys for 1093°C (2000°F) Turbine Blade Applications", NASA CR-159720, 1979.

2. D. W. Petrasek and R. A. Signorelli, "Tungsten Fiber Reinforced Superalloys - A Status Review", NASA TM-82590, 1981.

3. E. A. Winsa, "Tungsten Fiber Reinforced Superalloy Composite High Temperature Component Design Considerations", NASA TM-82811, 1982.

4. D. W. Petrasek, E. A. Winsa, L. J. Westfall and R. A. Signorelli, "Tungsten Fiber Reinforced FeCrAlY - A First Generation Composite Turbine Blade Material", NASA TM-79094, 1979.

5. E. A. Winsa, L. J. Westfall and D. W. Petrasek, "Predicted Inlet Gas Temperatures for Tungsten Fiber Reinforced Superalloy Turbine Blades", NASA TM-73842, 1978.

6. P. Melnyk and J. N. Fleck, "Tungsten Wire/FeCrAlY Matrix Turbine Blade Fabrication Study", NASA CR-159788, 1979.

7. W. D. Brentnall, "Metal-Matrix Composites for High Temperature Turbine Blades", TRW-ER-7790-F, TRW Inc., Cleveland, Ohio, 1976, and NADC-76225-30, Naval Air Development Center, Warminster, Pennsylvania, 1976.

8. C. C. Chamis, NASA Lewis Research Center, Cleveland, Ohio (unpublished notes).

9. J. E. Ashton, J. C. Halpin and P. H. Petit, Primer on Composite Materials: Analysis, Technomic Publishing Co., Inc., Stamford, Connecticut, 1969.

10. B. D. Agarwal and L. J. Broutman, Analysis and Performance of Fiber Composites, John Wiley and Sons, New York, 1980.

11. C. C. Chamis and G. P. Sendeckyj, "Critique on Theories Predicting Thermoelastic Properties of Fibrous Composites", J. Composite Materials, Vol. 2, No. 3, July 1968, pp. 332-358.

12. C. C. Chamis, "Simplified Composite Micromechanics Equations for Hygral, Thermal and Mechanical Properties", NASA TM-83320, 1983.

13. C. C. Chamis, "Simplified Composite Micromechanics Equations for Strength, Fracture Toughness and Environmental Effects", Proceedings of the "39th Annual Conference, Reinforced Plastics/Composites Institute", the Society of the Plastics Industry, Inc., January 16-20, 1984, Session 11-D, pp. 1-16.

14. C. C. Chamis, NASA Lewis Research Center, Cleveland, Ohio (unpublished notes).

15. A. C. Ugural, Stresses in Plates and Shells, McGraw-Bill Book Co., New York, 1981.

16. J. E. Ashton and J. M. Whitney, Theory of Laminated Plates, Technomic Publishing Co., Inc., Stamford, Connecticut, 1970.

17. C. W. McCormick, ed., "MSC/NASTRAN User's Manual", The MacNeal-Schwendler Corporation, Los Angeles, California, April 1982.

APPENDIX

APPENDIX

VALIDATION OF COMPOSITE MICROMECHANICS EQUATIONS

In the discussion of composite micromechanics theory in Chapter 2, equations were presented (see Figures 6-8) for predicting material properties of a unidirectional fiber-reinforced composite lamina based on the corresponding properties of the constituents of the lamina. The equations, as reported in references 12 and 13, were derived using a mechanics of materials approach for modelling the behavior of a composite material. The properties predicted by the composite micromechanics equations represent average values for an equivalent pseudo-homogeneous ply.

In order to assess the validity and accuracy of the composite micromechanics equations derived based on the mechanics of materials approach, a finite element study was conducted as alluded to in Chapter 2. The purpose of the study was to compare the predictions of mechanical properties ($E_{\ell 11}$, $E_{\ell 22}$, $G_{\ell 12}$, $G_{\ell 23}$, $\nu_{\ell 12}$, and $\nu_{\ell 23}$) and thermal properties ($\alpha_{\ell 11}$ and $\alpha_{\ell 22}$) from the micromechanics equations with the average values simulated in a finite element structural analysis.

The finite element model used for the study is shown in Figure 33 and is intended to represent a single, continuous, unidirectional fiber imbedded in a square array of matrix with an interphase of material existing at the fiber/matrix boundary. The discretized finite element model was comprised of 125 nodes and 96 three-dimensional isoparametric "brick" elements. This model is consistent with the basic composite element assumed in the mechanics of materials approach used to derive the composite micromechanics equations.

In conducting the finite element study, the MSC/NASTRAN code (ref. 17) was used for the structural analyses. In short, through careful application of the loading and boundary conditions, it was possible to simulate such modes of deformation as pure extension or pure shear. By applying simple equations of mechanics (see Figure 33) in conjunction with the results of the finite element analysis, it was possible to calculate the simulated average material property values for the model as a whole resulting from the combined effect of the individual elements. The material property values determined in this way were then compared to the values predicted by the corresponding composite micromechanics equations.

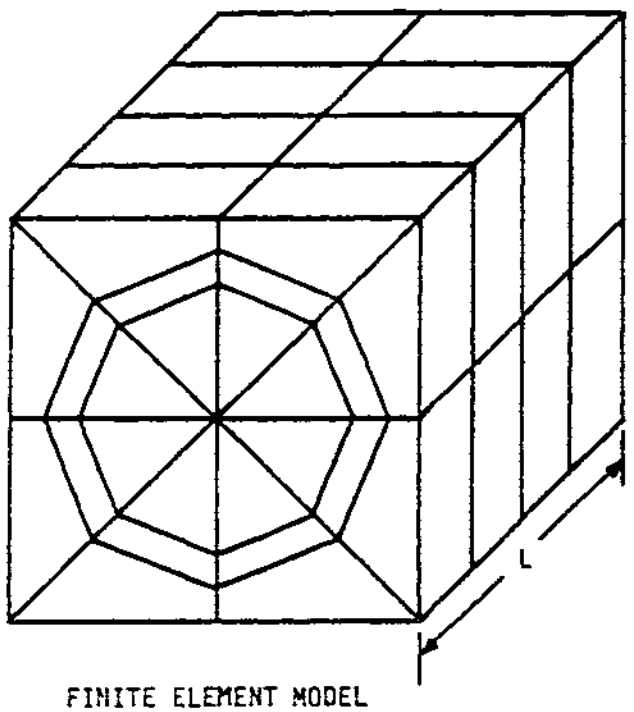

FINITE ELEMENT MODEL

(a) Finite Element Model

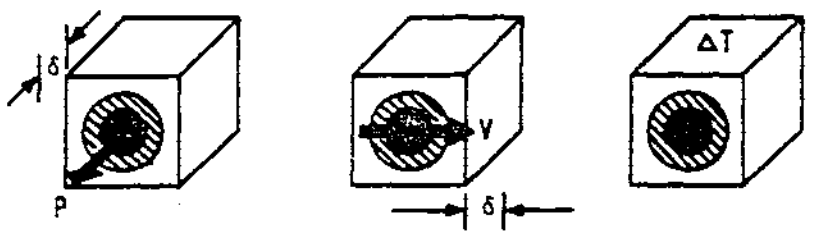

$E = \frac{PL}{A\delta}$ $G = \frac{VL}{A\delta}$ $\alpha = \frac{\delta}{(\Delta T)L}$

(b) Mechanics of Materials Equations

Figure 33 - Composite Model and Mechanics of Materials Equations for Composite Micromechanics/FEM Validation Study

The results of the composite micromechanics/finite element validation study are summarized in Table 3. Comparison of the results indicates excellent agreement between the corresponding values of material properties determined by the two methods. Based on these results, it was concluded that the underlying principles and assumptions inherent in the mechanics of materials approach to composite material modelling are reasonable and realistic. Furthermore, it was concluded that the equations derived by the mechanics of materials approach could be used with confidence in the nonlinear analysis of a TFRS composite turbine blade/vane structure.

Table 3 - Comparison of Ply Properties from Composite Micromechanics/FEM Validation Study

PROPERTY	UNITS	MICROMECHANICS PREDICTION	FEM ANALYSIS
$E_{\ell 11}$	10^6 psi	37.2	37.2
$E_{\ell 22}$	10^6 psi	35.7	35.3
$G_{\ell 12}$	10^6 psi	13.8	14.3
$G_{\ell 23}$	10^6 psi	13.8	14.0
$\nu_{\ell 12}$		0.30	0.30
$\nu_{\ell 23}$		0.30	0.28
$\alpha_{\ell 11}$	10^{-6} in/in/^{o}F	4.0	4.0
$\alpha_{\ell 22}$	10^{-6} in/in/^{o}F	5.0	4.3

1. Report No.	2. Government Accession No.	3. Recipient's Catalog No.
NASA TM-83754		

4. Title and Subtitle	5. Report Date
Nonlinear Analysis for High-Temperature Multilayered Fiber Composite Structures	August 1984
	6. Performing Organization Code: 505-33-5B
7. Author(s): Dale A. Hopkins	8. Performing Organization Report No.: E-2242
	10. Work Unit No.
9. Performing Organization Name and Address: National Aeronautics and Space Administration, Lewis Research Center, Cleveland, Ohio 44135	11. Contract or Grant No.
	13. Type of Report and Period Covered: Technical Memorandum
12. Sponsoring Agency Name and Address: National Aeronautics and Space Administration, Washington, D.C. 20546	14. Sponsoring Agency Code

15. Supplementary Notes

This report was submitted as a thesis in partial fulfillment of the requirements for the degree Master of Science in Civil Engineering to The University of Akron, Akron, Ohio in May 1984.

16. Abstract

A unique "upward-integrated top-down-structured" approach is presented for nonlinear analysis of high-temperature multilayered fiber composite structures. Based on this approach, a special purpose computer code was developed (nonlinear COBSTRAN) which is specifically tailored for the nonlinear analysis of tungsten-fiber-reinforced superalloy (TFRS) composite turbine blade/vane components of gas turbine engines. Special features of this computational capability include accounting of; micro- and macro-heterogeneity, nonlinear (stress-temperature-time dependent) and anisotropic material behavior, and fiber degradation. A demonstration problem is presented to manifest the utility of the upward-integrated top-down-structured approach, in general, and to illustrate the present capability represented by the nonlinear COBSTRAN code. Preliminary results indicate that nonlinear COBSTRAN provides the means for relating the local nonlinear and anisotropic material behavior of the composite constituents to the global response of the turbine blade/vane structure.

17. Key Words (Suggested by Author(s))	18. Distribution Statement
Nonlinear analysis; Fiber composites; Material nonlinearities; Finite element analysis; Turbine blades/vanes; High-temperature composites	Unclassified - unlimited STAR Category 24

19. Security Classif. (of this report)	20. Security Classif. (of this page)	21. No. of pages	22. Price*
Unclassified	Unclassified		

*For sale by the National Technical Information Service, Springfield, Virginia 22161

END

DATE

FILMED

DEC 23 1985